SANDIA REPORT SAND84-8251 • Unlimited Release • UC-62d
Printed December 1984

Solid Particle Receiver Experiments: Radiant Heat Test

J. M. Hruby, B. R. Steele, and V. P. Burolla

Prepared by
Sandia National Laboratories
Albuquerque, New Mexico 87185 and Livermore, California 94550
for the United States Department of Energy
under Contract DE-AC04-76DP00789

SF 2900-Q(6-82)

Issued by Sandia National Laboratories, operated for the United States Department of Energy by Sandia Corporation.

Printed in the United States of America
Available from
National Technical Information Service
5285 Port Royal Road
Springfield, VA 22161

NTIS price codes
Printed copy: A05
Microfiche copy: A01

UC-62d

SAND84-8251
Unlimited Release
Printed December 1984

SOLID PARTICLE RECEIVER EXPERIMENTS: RADIANT HEAT TEST

J. M. Hruby
B. R. Steele
V. P. Burolla

Solar Components Division
Sandia National Laboratories, Livermore

ABSTRACT

In tests designed to simulate the fundamental characteristics of a solar thermal solid particle central receiver, a continuous stream of free-falling particles has been heated to temperatures in excess of 1300 K over a ten meter fall height in the presence of a radiant flux of 0.50 MW/m^2. The ability to heat particles to temperatures this high is a major step in demonstrating the technical feasibility of the solid particle receiver concept. Particle temperatures were varied by altering mass flow rate, incident radiant flux, and particle size and optical properties. Flux levels were varied between 0.10 and 0.50 MW/m^2 for silicon carbide and silica sand particles with nominal sizes of 300 μm, 500 μm and 1000 μm. Particle generated convection currents increased particle residence times by as much as a factor of three. No particle sintering effects were observed.

CONTENTS

ILLUSTRATIONS

TABLES

SUMMARY

This is the second in a series of reports concerning tests designed to evaluate the solar thermal solid particle receiver concept. The focus of the present report is an experiment performed at the Radiant Heat Facility, Sandia National Laboratories, Albuquerque. In this experiment, a continuous stream of free-falling particles was irradiated over a ten meter fall height. The radiant source employed was a series of tungsten filament quartz lamps. The lamps provided a repeatable and reliable incident radiant flux at selected levels between 0.1 and 0.6 MW/m^2.

Because the solid particle receiver is being studied as a high-temperature receiver concept, the objective of this experiment was to determine if particles could be heated to temperatures greater than 850 K in reasonable fall distances and with moderate incident fluxes for solar central receivers (current generation central receivers are 10 to 20 m in height and receive an incident flux 0.3 to 0.6 MW/m^2). In addition, functional relationships were desired between particle heating and particle characteristics such as optical properties and size. The relationship between incident flux, initial particle temperature, and initial particle dispersion was also desired. These relationships were needed for analytical model verification as well as receiver design tools.

A major step in demonstrating the technical feasibility of the solid particle receiver concept was taken by heating particles to temperatures in excess of 1300 K in the presence of a radiant flux of 0.5 MW/m^2. In addition, functional relationships desired for analytical model verification and receiver design were established. Particle temperature was seen to be dependent on particle absorptivity and residence time. Particle temperature increases as flux is increased; however, in this experiment the rate of increase slowed as the flux increased beyond approximately 0.4 MW/m^2. A simple model to describe the relationship between particle heating and other parameters was developed.

Hot particles heating the surrounding air generated convective currents which decreased particle velocities as much as 5 m/s. This decrease in particle velocity

indicates that convection currents could be significant in a high-temperature solid particle receiver. Convection can be used to increase the residence time of the particles, and shorten the required receiver height to achieve a desired temperature. This is advantageous because convective losses decrease as the cavity size decreases. Silica sand and silicon carbide particles with sizes of 500 or 1000 μm did not fracture or sinter after multiple cycles in the radiant flux.

SOLID PARTICLE RECEIVER EXPERIMENTS: RADIANT HEAT TEST

INTRODUCTION

This is the second in a series of reports concerning experiments designed to evaluate the solid particle receiver concept. In this concept, particles free-fall in a cavity central receiver and directly absorb the incident solar radiation. The solid particle receiver is being studied for high performance, high temperature applications of solar energy. For a description of the concept and experiments previously conducted see References [1] and [2].

The solid particle receiver program is in a technical feasibility phase. As part of the current study, analytical aerodynamic and thermal modeling and associated experimental investigations are being conducted. Other activities are also underway, such as studies on the sinter and fracture characteristics of particles. This report presents an experiment in which free-falling particles were irradiated with infrared lamps over a ten meter fall distance. The intensity of the lamps was comparable to the solar flux at a central receiver, but spectrally different. This radiant heat experiment serves two purposes: it provides engineering information concerning particle aerodynamic and thermal behavior, and provides data for analytical model verification.

TEST DESCRIPTION

Objectives

The experiment and apparatus described herein were designed with several objectives in mind. Specific functional relationships were desired between particle heating and particle characteristics such as optical properties and size. The effect of

mass flow, velocity, initial temperature, initial dispersion and incident radiant flux on final particle temperature was also of interest. Another phenomena of importance was convective losses from the hot chute walls and hot particles.

This test was also aimed at proving the concept behind a solid particle receiver, namely that particles falling a distance equivalent to that obtainable in existing solar central receiver designs could be heated to temperatures in excess of 850 K by a nominal radiant flux (current central receivers designs are 10 to 20 m in height with incident flux levels between 0.3 and 0.6 MW/m^2). The particles used in this experiment were the size and kind that would function in a solid particle receiver. Previous studies [1] have indicated that refractory particles with a diameter between 100 μm and 1000 μm were the most likely candidates.

Facility and Apparatus

The major components of the test apparatus were an insulated chute, a bank of tungsten filament infrared lamps, a particle discharge hopper, and a particle catch bin. The chute was a three-walled, rectangular sheet metal structure lined with 2.5 cm thick fiberfrax refractory. There were four 2.44 m sections individually attached to two ten meter long steel angle irons. An illustration of the apparatus is shown in Figure 1. Gaps existed between the chute sections to allow for thermal expansion and were filled with ceramic blanket insulation so that the entire ten meter height was a continuous insulating surface. The chute internal cross section was 0.15 m deep by 0.30 m wide. The fourth side of the chute was designed to admit the radiant flux and confine the particles within the chute. It consisted of a series of fused silica plates 0.30 m square. These silica plates were held in sets of four by metal brackets attached to the infrared lamp holders. The brackets were positioned to allow expansion of the plates or brackets to overlap so that there were no gaps to allow the falling particles to escape from the chute. Deflectors made with refractory material were attached to the side of the chute to cover the 2.5 cm

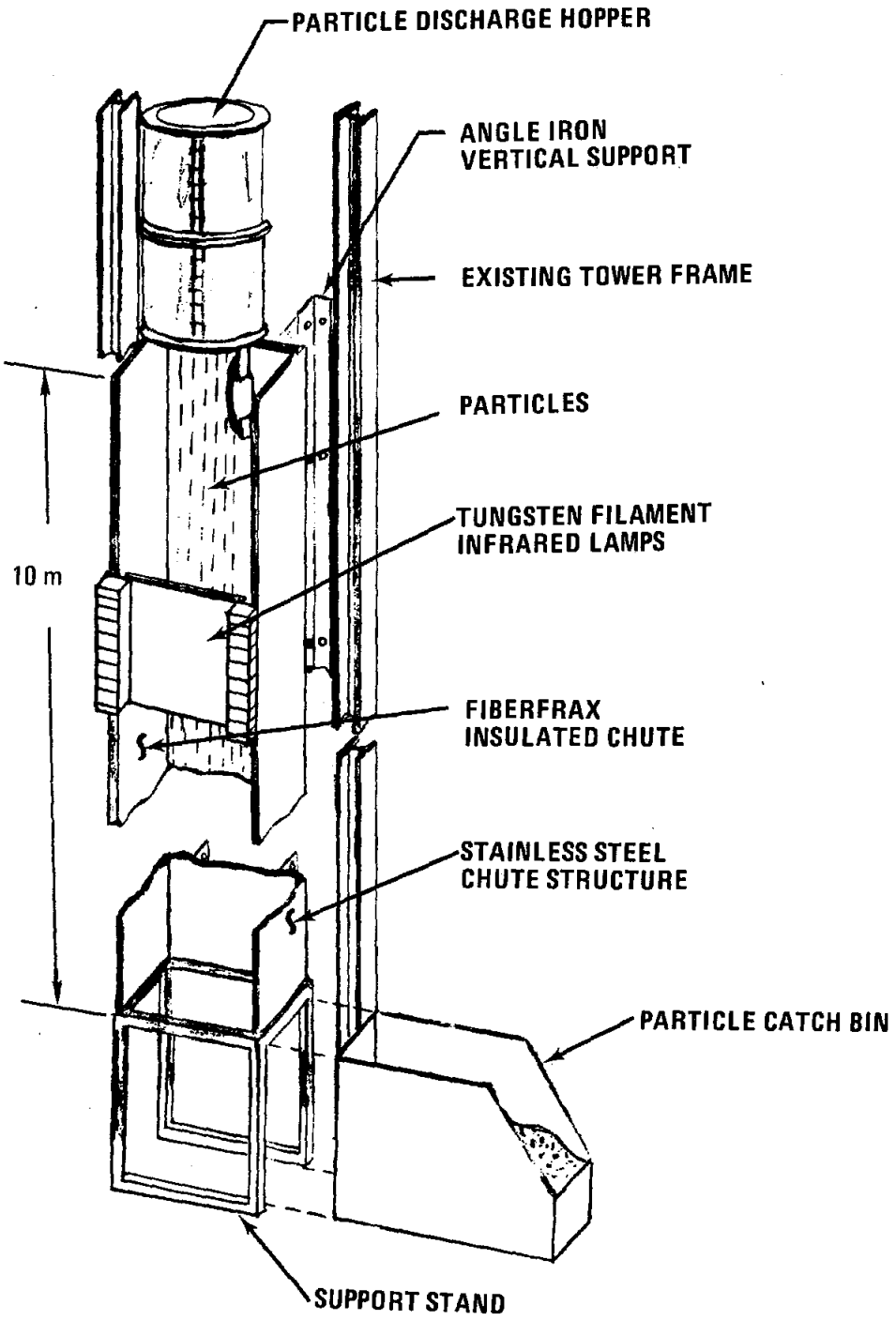

Figure 1. Illustration of Test Apparatus

gap between the silica plates and the front of the chute.

The infrared lamps supplying the radiant flux were mounted horizontally on water-cooled, polished aluminum reflectors that were adjacent to the silica plates. A photograph of the lamps mounted on the aluminum reflectors is shown in Figure 2. The lamps were stacked vertically along each reflector, and the reflectors were stacked vertically to create a radiant source 10 m high and 0.30 m wide. A total of 334 lamps and eight aluminum reflectors were used.

Particle flow into the chute was controlled by varying the size of slits machined into the bottom of the discharge hopper which was located 0.3 m above the chute. In some cases this meant changing the bottom plate in the discharge hopper, and in other cases it meant allowing flow through slits which had originally been blocked. An artist's rendition of the top of the test apparatus with the discharge hopper dispersing particles into the chute is shown in Figure 3. The top of the chute was fitted with a sheet metal rectangular funnel that deflected vertical air currents to allow the particles to enter the chute virtually undisturbed from the initial curtain configuration. (Note: after about one meter of fall the particle curtain is completely dispersed and fills the entire chute cross section, unlike the conditions at inlet.) The discharge hopper was capable of preheating the particles to 850 K using ceramic band heaters. This capability was added to study the effects of particle generated convection currents. An air operated vibrator attached to the base of the discharge hopper provided nearly uniform particle discharge rates.

The heated particles were collected in a thin walled insulated sheet metal bin designed to allow the entrained air in the particle flow to escape, while not absorbing a significant amount of heat from the particles.

The entire apparatus was mounted on a tower at the Radiant Heat Facility, Sandia National Laboratories, Albuquerque. The tower and associated hardware, having been constructed for previous tests, provided connections to cooling water, power, and data acquisition systems while also permitting personnel access at several levels. Cooling fans were installed on each level to blow air between the silica plates and the infrared lamps to allow the lamps to operate at levels above 0.3 MW/m^2 for

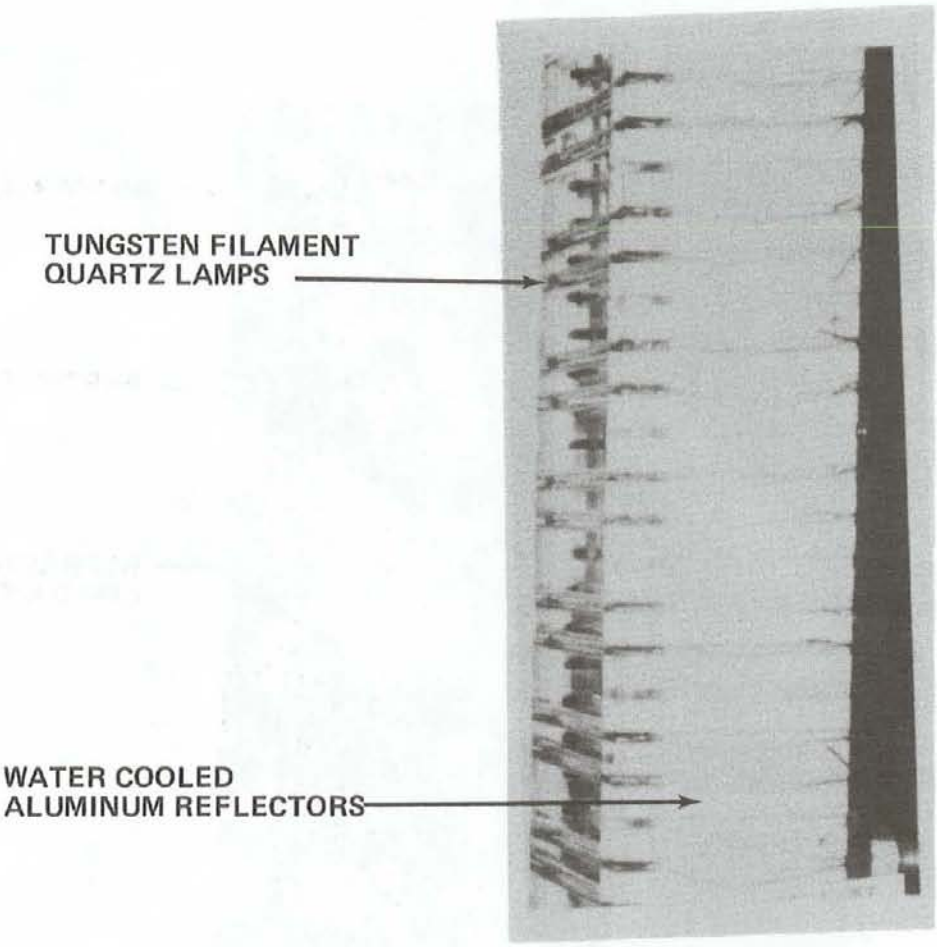

Figure 2. Photograph of Tungsten Filament Lamps Mounted on Water-Cooled Aluminum Reflectors

extended periods. A lifting platform was positioned immediately adjacent to the tower to elevate a laser Doppler velocimetry system to the proper vertical position for particle velocity measurements within the chute. A photograph of the tower and apparatus is shown in Figure 4.

The geometry chosen was governed by the existing tower configuration. No attempt was made to optimize the performance of the apparatus since it was realized early that the chute did not represent a geometry that would be used in a solid particle receiver. Similarly, the tungsten filament lamps were used to allow greater

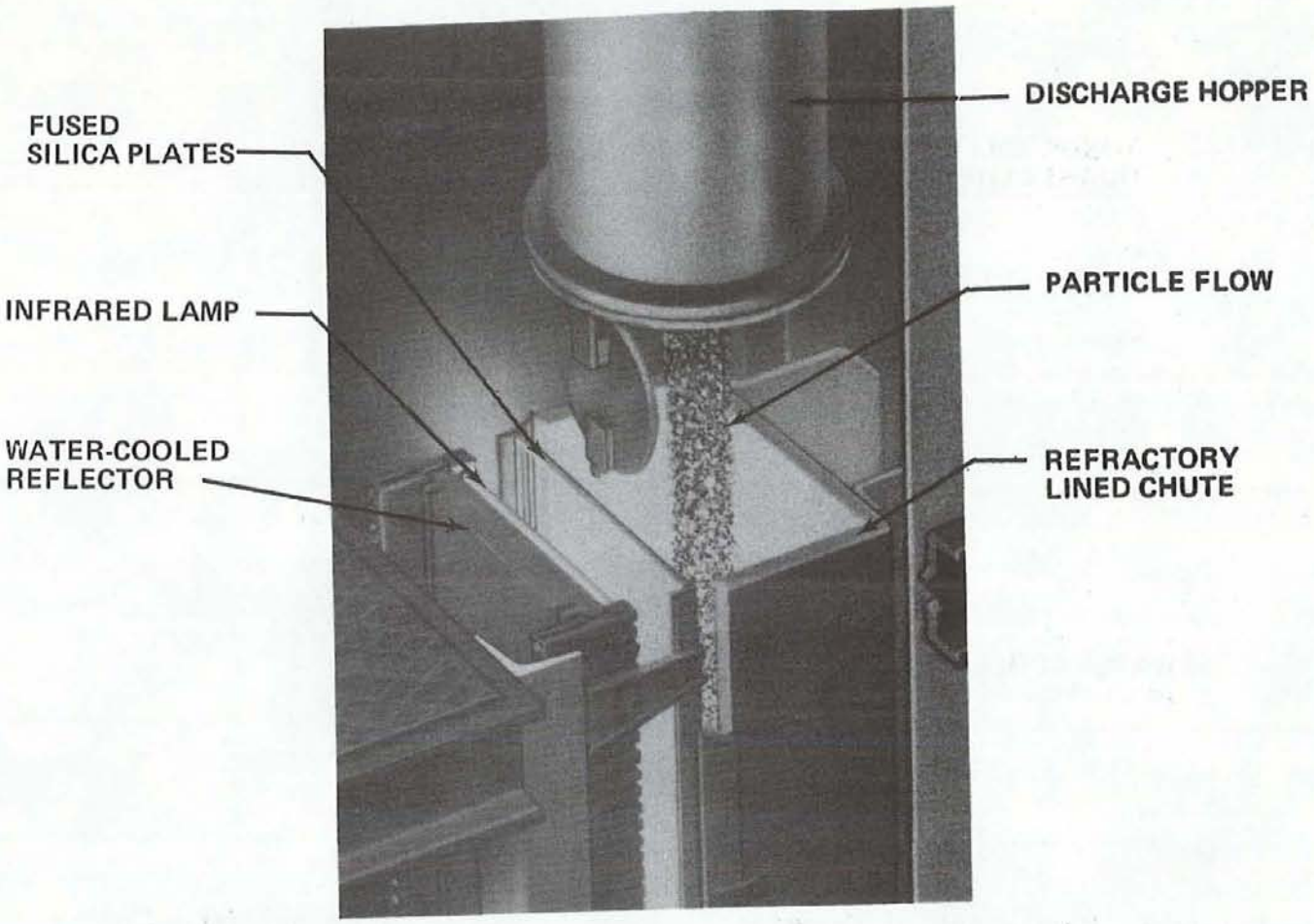

Figure 3. Artist's Rendition of Top of Chute

control over test parameters and greater reliability than a solar flux would permit.

Two materials were used in this experiment so that a range of size and absorptance could be examined. The two particle materials chosen were silicon carbide and silica sand. Silicon carbide and silica sand were chosen specifically because their optical properties are different from one another, and they are inexpensive

Figure 4. Photograph of Experimental System at Radiant Heat Facility

and readily obtainable in large quantities. The measured absorptance of silicon carbide was nearly constant over a weighted solar and infrared spectra at 0.83 and 0.84 respectively, while the measured absorptance of the silica sand was 0.68 for the weighted solar and 0.62 for the weighted infrared (see Appendix A). Based on studies done at Pennsylvania State University, both materials were expected to maintain their flowability in the estimated temperature range [3]. The silicon carbide particles were nominally 300 μm, 500 μm and 1000 μm, while the silica sand particles were nominally 300 μm and 1000 μm. Detailed size distribution for 500 μm silicon carbide particles and 300 μm silica sand particles is included in Table 1. Typically, at least 70 percent of the particles are larger than the nominal size with less than ten percent larger than 1.6 times the nominal size. The variance about the mean is expected to be similar for other size silicon carbide and silica sand particles. The particles were not discarded after each test but rather cooled, sifted to remove debris, and used again.

Diagnostics

Temperature data was acquired with chromel alumel, sheathed, ungrounded thermocouple probes located in the discharge hopper, along the inside and outside walls of the chute as well as within the insulation, and in the catch bin. For in-situ particle temperature measurements, a small insulated bucket attached to the end of a pole and instrumented with a thermocouple was inserted into the particle flow until the bucket was filled and the thermocouple recorded particle temperature. This method for particle temperature measurement has been proven by others to be reliable [4]. The probe was inserted into the chute through 5 cm diameter access holes.

The particle discharge hopper was suspended from three load cells. These load cells recorded the mass flow rate of particles. The cells were instrumented with thermocouples to insure that the readings were not being perturbed by temperature

Table 1. Particle Volumetric Size Distribution

(a) 500 μm Silicon Carbide

Size (μm)	*Percent by Volume*
> 1000	0.0
$840 - 1000$	0.0
$710 - 840$	10.9
$600 - 710$	74.2
$500 - 600$	13.5
$420 - 500$	1.2
$350 - 420$	0.0
$300 - 350$	0.0
< 300	0.2

(b) 300 μm Silica Sand

Size (μm)	*Percent by Volume*
> 704	0.0
$500 - 704$	6.9
$352 - 500$	38.0
$250 - 352$	38.5
$176 - 250$	15.7
$125 - 176$	0.1
< 125	0.7

variations.

Radiant flux data came from four circular foil heat flux gages, one gage in each chute section. The absorbing surface of each flux gage was mounted flush with the rear wall at the midpoint of each chute section. Spectral flux data was acquired using a pyroelectric radiometer and a series of narrow band infrared interference filters. Spatial flux data was obtained with a circular foil heat flux gage enclosed in a water-cooled jacket. The spectral and spatial flux measurements were done on a fifth chute section located in a laboratory near the test tower.

Particle velocity measurements, necessary to calculate particle residence time in the flux, were accomplished with a laser Doppler velocimetry (LDV) system mounted on a lifting platform adjacent to the tower. The LDV system employed standard TSI Incorporated optics and processing electronics connected to an HP 9826 computer through a custom interface. The focal length of the final positive lens in the backscatter LDV system was 2.2 m. This focal length provided adequate distance between the optics and the radiant source to avoid excessive heating of any component. The receiving optics were equipped with a ten nanometer bandpass laser line filter to eliminate infrared radiant flux and extraneous light in the photomultiplier. A Lexel 4 W argon ion laser provided the 514.5 nanometer light source. The laser, power supply, and optics were covered by a sheet metal enclosure for protection from the elements. A detailed discussion of the LDV system is included in Reference [2]. The laser beams entered the chute through 5 cm diameter access ports in the rear wall of the chute.

All temperature, flux gage, and load cell channels were scanned every ten seconds during a test. Particle velocity data acquisition was often slow and so, in most cases, particle velocity data was collected only once during a run to obtain a large enough population sample for meaningful statistical analysis. A sample with a population of 50 was considered the absolute minimum. In some cases, however, velocity data acquisition was rapid enough to obtain several sets of data in one run.

In many cases, lamp voltage and current were recorded as a check on the reproducibility of lamp radiant output.

BASELINE CHARACTERIZATION TESTS

Cold Flow Velocity Profile

Cold flow velocity data was collected to establish a baseline for comparison to hot flow velocities. Any difference between cold flow and hot flow velocities is indicative of convective air movement.

In the cold flow velocity profile tests, the radiant lamps were not used but all components of the system were in place. The only data acquisition used was the LDV system. The flow rate for each slit arrangement was measured and assumed to be unchanged throughout the testing. Prior to initiating particle flow, the vibrator at the base of the discharge hopper was turned on, the LDV platform moved to the appropriate position and the laser beams directed into the chute. When particle flow started the LDV system was adjusted (if necessary) until a valid signal and acceptable data rate was obtained. At that point, velocity data acquisition began. In some cases, the data rate was high enough to permit several 500 count data sets. Velocity measurements were made at 0.1 m, 1.77 m, 4.01 m, 6.66 m and 9.80 m from the bottom of the discharge hopper and approximately in the center of the chute cross section.

The cold flow data, presented in Figure 5, compares well with data from previous experiments [2]. The 1000 μm silicon carbide and silica sand particles had virtually identical cold flow velocity profiles (velocity profile in this report refers to velocity as a function of distance of fall) with the exception of the measurement for silica sand at 4.11 m. Because of the similarity in the shapes of the two profiles and the agreement with the other data points, this single point is considered to be an anomaly. The optical properties of the silica sand made measurements difficult and more susceptible to errors. The particles do not appear to have reached terminal velocity after ten meters of fall in any test.

In two tests, the LDV system was positioned 0.1 m below the discharge hopper.

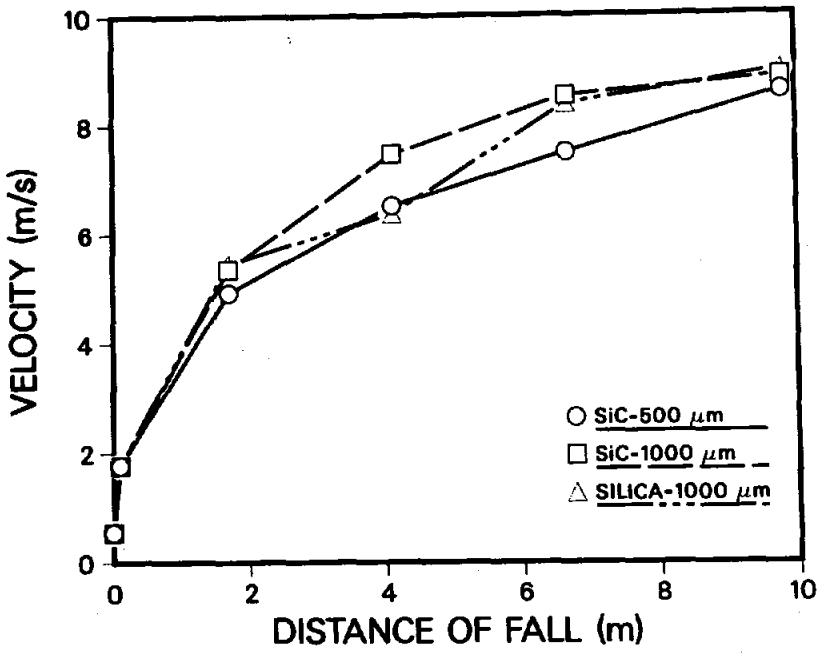

Figure 5. Particle Velocity Profile in Chute without Flux

A velocity of 1.77 m/s was measured for 500 μm and 1000 μm silicon carbide particles. The data varied by 0.001 m/s, indicating that aerodynamic effects were not present at this distance. Therefore, the particle velocity at short distances is only a function of the slit exit velocity and acceleration due to gravity. A slit exit velocity of 0.55 m/s was calculated for this test based on the measurements made at 0.1 m. This value was used for all tests.

Spectral Flux Characterization

Spectral flux measurements were necessary in this experiment because the radiant spectrum of the infrared lamps was unknown. In order to use the results of this experiment to describe the behavior of a solar solid particle receiver, the spectral characteristics of the lamps and particles must be well understood. It was also important to establish whether any elements of the chute were perturbing the lamp spectral output.

Spectral flux measurements were not done on the full scale chute but on one chute section located in an adjacent laboratory. A 5 cm diameter hole had been cut in the chute rear wall to allow the radiant lamps to be viewed. The measurements were made with a pyroelectric radiometer mounted on a plate along with a filter wheel capable of holding 18 filters. The radiometer and filter wheel were aligned with the opening in the rear wall of the chute. The radiometer was calibrated and stabilized for at least two hours prior to the test.

When the lamps were on, the radiometer was shielded by reflective insulation from any flux except when measurements were taken. The insulation was removed only as long as necessary to obtain a stable reading from the radiometer, which usually took less than 30 s. The data was taken when the chute walls had reached a steady temperature. This temperature corresponded to the wall temperature normally obtained prior to particle flow in the full scale experiments. Flux levels with no filter present were recorded just prior to and just after the flux levels with filters. At each incident flux level of interest, at least two sets of measurements were taken. One data set was taken by starting with the lowest mean wavelength filter and taking progressive readings until the highest mean wavelength measurement was complete. The other data set was completed by moving from highest to lowest wavelength. This allowed the effects of time (non-steady state) to be evaluated. The chute was allowed to cool before proceeding to the next incident flux level of interest. Cooling was allowed to insure correct simulation of the conditions in actual particle flow tests.

The measured spectral flux curve for a flux level of 0.25 MW/m^2 had the shape of a blackbody spectrum. Furthermore, the area under the measured flux curve agreed with the total flux measurements (with no spectral filter), indicating that there was not a significant amount of energy at wavelengths longer or shorter than those measured. Therefore, the peak wavelength was found by superimposing a calculated blackbody curve on the measured curve. The best fit of the blackbody and measured curve indicated the peak wavelength of the lamps. The peak wavelength of the lamp spectrum was determined to be 1.17 μm for an incident

radiant flux of 0.25 MW/m^2. The filament temperature can be deduced knowing the peak wavelength of the blackbody curve by employing Wien's displacement law, $\lambda_{max}T = 2898\ \mu mK$.

There was a slight shift in the peak wavelength at various intensity levels. This shift can be predicted by describing the emissivity of the tungsten filament as a function of temperature and assuming that $q \sim \epsilon T_f{}^4$, where T_f is the filament temperature, and ϵ the lamp emissivity. (This assumption implies that the heat flux is a function of the tungsten filament only and not the chute walls, etc.) The emissivity of a tungsten filament is proportional to $T_f - 5.88$ [5].

In this case, therefore, $q \sim (T_f - 5.88)T_f{}^4$. Since the peak wavelength of the lamps is known for 0.25 MW/m^2, a ratio of heat fluxes and temperatures can determine the peak wavelength shift at other flux intensities. For example, the tungsten filament temperature at 0.4 MW/m^2 can be determined from the ratio

$$\frac{0.25}{0.4} = \frac{(T_{f,0.25} - 5.88){T_{f,0.25}}^4}{(T_{f,0.4} - 5.88){T_{f,0.4}}^4}$$

In this case, $T_{f,0.4}$ is 2708 K, and the corresponding peak wavelength 1.07 μm. Likewise, the peak wavelength for 0.50 MW/m^2 can be calculated to be 1.02 μm.

Figures 6, 7 and 8 compare the blackbody curve for the predicted peak wavelength with the measured spectral flux curve. The comparison is quite good for all flux levels, but the most significant deviation occurs at the lowest peak wavelength (highest temperature). At a flux level of 0.50 MW/m^2, the blackbody spectrum falls below the measured spectrum at wavelengths longer than the peak wavelength. This low curve indicates that infrared emission, from the quartz envelope surrounding the lamps and chute walls, is more significant at higher incident flux and temperature levels. These variations are small enough to neglect in calculations requiring a spectral flux input.

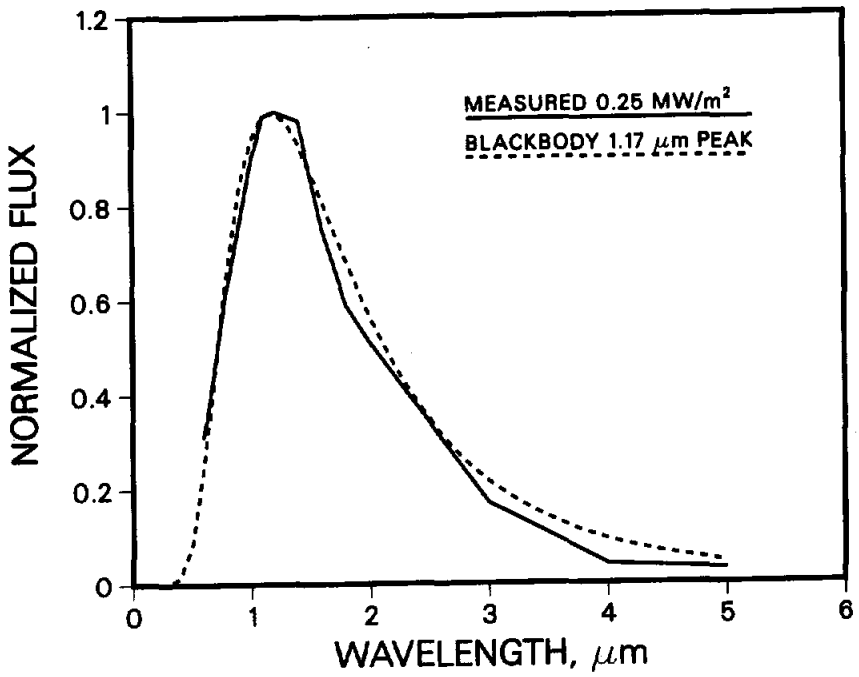

Figure 6. Measured Spectral Flux Distribution for 0.25 MW/m^2

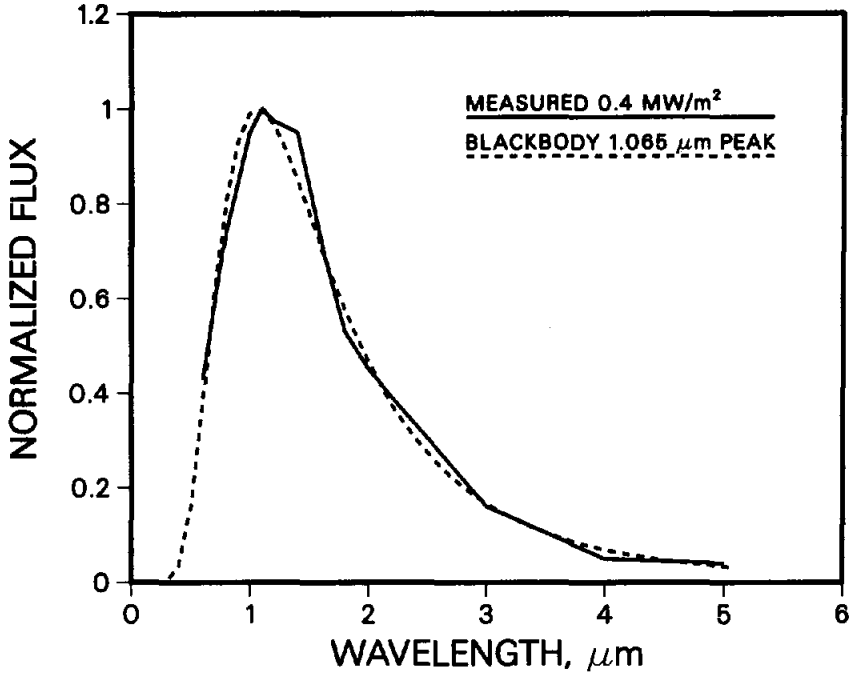

Figure 7. Measured Spectral Flux Distribution for 0.4 MW/m^2

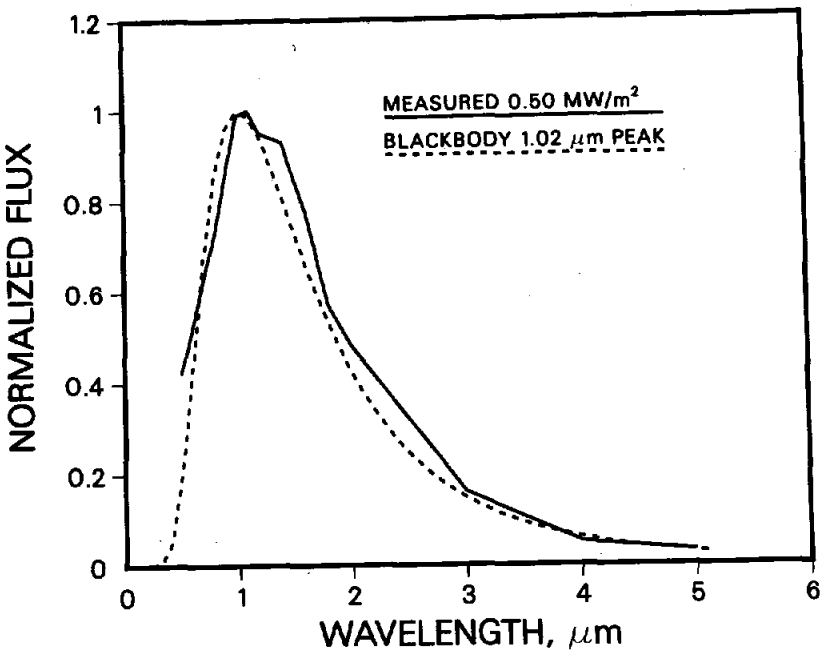

Figure 8. Measured Spectral Flux Distribution for 0.5 MW/m^2

Spatial Flux Distribution

A three-dimensional mapping of the radiant flux (Appendix C) was necessary to establish the uniformity of the flux with all elements of the chute in place. These measurements were accomplished on the same chute section used for the spectral flux measurements, but with a specially designed water cooled heat flux probe that could be inserted into the chute. The back of the chute had an "H" shaped cutout to allow probe movement horizontally and vertically. In all cases, the absorbing surface of the probe was kept parallel to the plane of the lamps. By moving the probe in three directions, a spatial flux distribution was obtained. All data was taken when the chute conditions were stabilized, i.e. flux and temperature did not vary significantly with time. The flux was found to vary by as much as 30 percent of the peak value with chute width (side-to-side) and less than 5 percent with chute depth (front-to-back), see Figure 9. The flux was constant in the vertical direction.

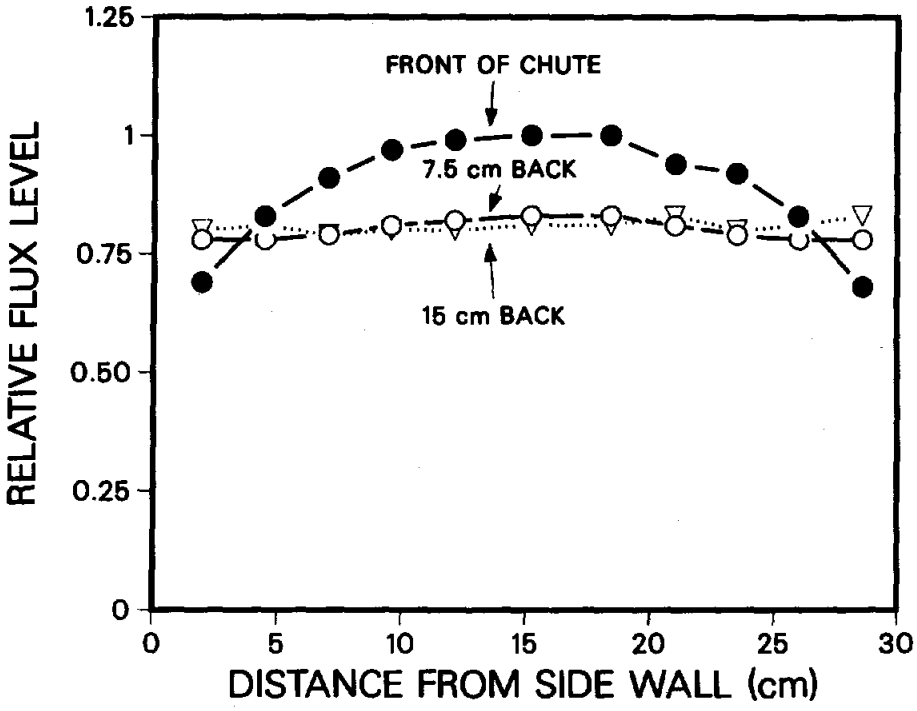

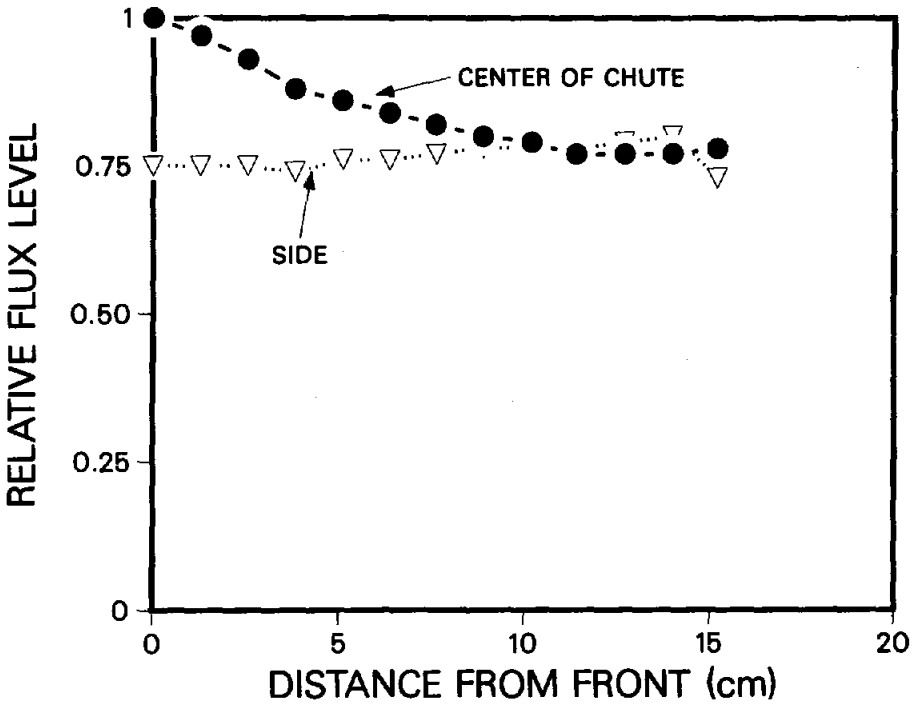

Figure 9. Measured Spatial Flux Distributions

RADIANT HEATING TESTS

Procedures

Series 400: Preliminary Flux Tests

For these tests the LDV system was not used and some of the thermocouples in the discharge hopper and catch bin were not in place. Test procedures were varied somewhat to determine the optimum flow rate of particles, the temperature response of the load cells and the effects of chute preheat. The flow rate was considered optimum when the particles quickly filled the chute and an appropriate amount of flow time and heating occurred. For some of the tests particle flow (with the vibrator on) was initiated just after the lamps reached full test voltage, and in other tests particle flow started prior to the lamps being energized. Flux levels varied between 0.15 MW/m^2 and 0.25 MW/m^2. Mass flow rates varied between 6 kg/min and 14 kg/min.

Series 450: Steady State Flux Tests

For this series, the LDV system was used and the lamps energized prior to particle flow. Particle flow was initiated when the chute wall temperature was nearly invariant with time. For consistency, a specific thermocouple on the back inside chute wall was monitored. The chute wall temperature was assumed to be in steady state when this thermocouple reached 830 K.

There were six thermocouples monitoring hopper temperature (initial particle temperature) and six thermocouples staggered vertically in the catch bin. The vertical arrangement of thermocouples in the catch bin enabled the generation of a time-final particle temperature plot.

The LDV system was in place prior to the start of the run and in some cases a short duration cold flow test of the LDV system was made. Once the particle flow

for the actual test began, the LDV system was adjusted until an acceptable data rate was obtained and then the data taken.

For tests 452 and later, the load cells were thermally insulated and cooled with a blower. These precautions minimized the temperature rise of the load cells to less than 10 K during a run to insure correct measurements. All tests in this series used a 64 mm by 6 mm slit to discharge particles in the chute. No in-situ particle temperature measurements were attempted. In most cases, particle flow ended before the lamps were turned off.

Series 500: Baseline Flux Tests

The chute preheat temperature for this series remained at 830 K and the discharge orifice was a single 64 mm by 6 mm slit except for test 501 which used two separate 32 mm long slits. LDV data acquisition was the same as series 450. In some tests, in-situ particle temperature measurements were made. If the location of the particle temperature probe was above the location for LDV data, the particle temperature data was not taken until after the LDV data. In some tests, a water-cooled heat flux probe was used to measure the spatial flux distribution during particle flow. As with the particle temperature probe, LDV data was taken at a location above this probe if the probe was protruding into the chute. 500 μm and 1000 μm silicon carbide particles and 1000 μm silica sand particles were used in this series. For tests 514 and 514A, only the top half of the lamp bank was turned on.

Series 600: Preheated Particles

In this test series no radiant flux was used; rather the particles were preheated and dropped in ambient air. The particles were heated in an oven, transferred to an insulated bin, transported to the top of the tower, and loaded into the preheated discharge hopper. During this process the particle temperature dropped 10 K. LDV data was taken along with in-situ and final particle temperature. 500 μm silicon

carbide particles were used for all tests.

Series 700: Optically Dissimilar Particles

The test procedure for this series was identical to the 500 series except that only 300 μm and 1000 μm silica sand was used. The LDV system was unable to acquire particle velocity data for the 300 μm particles.

Series 800: Varying Curtain Geometry

The test procedure for this series was identical to the 500 series except that a different orifice plate was used to distribute the particles into the chute. The plate consisted of slits at the bottom of tapered sides, thereby creating a higher initial velocity out of the discharge hopper. Two slit arrangements were used: (1) 3.2 mm by 483 mm, and (2) 3.2 mm by 228 mm.

Data Summary

All of the temperature, mass flow and incident flux data for radiantly heated or preheated particles are summarized in Table 2. The temperature data were reduced by noting the time in the test when the particle temperature in the catch bin reached its highest value, and retrieving all other temperature data at that same time. The tests in the 400 series were designed to establish steady state operating conditions for remaining tests and to correct any data acquisition deficiencies. As a result of the series 400 tests, the chute walls were allowed to preheat to approximately 830 K under full test flux prior to initiating particle flow. These preheated conditions assured the variation in flux gage readings was less than five percent over any two minute interval in the test.

Early in the testing, it became apparent that the 300 μm particles would not be suitable for data acquisition because more than half of the particles were carried out of the chute by convection currents. Therefore, most tests were conducted with

Table 2. Temperature, Radiant Flux, and Mass Flow Data Summary

Test (#)	Mat'l	Size (μm)	Flow (kg/min)	Total Flux No Flow[a] (MW/sq. m.)	Total Flux Full Flow (MW/sq. m.)	Temperatures Init (K)	Temperatures Particle Final (K)	Temperatures Change (K)	Temperatures Wall (K)	% Lamps ON
401[c]	SiC	300	UNK	.08	.05	285	825	540	400	u
402[c]	SiC	300	UNK	.00	.00					
403[c]	SiC	300	8.4[d]	.14	.09	280	990	710	515	u
404[c]	SiC	300	13.1	IND	.13	285	445	160	415	u
405	SiC	500	14.0	.10	.08	280	665	385	300	u
406	SiC	500	12.1	.21	.13	280	880	600	315	u
407	SiC	500	7.2	.28	.22	285	1135	850	620	u
408	SiC	500	UNK	.28	.23	425	1120	695	540	u
451	SiC	500	6.7	.29	.23	280	1155	875	860	u
452	SiC	500	6.5	.27	.22	280	1135	855	790	u
453	SiC	500	7.2	.25	.19	280	1110	830	750	u
454	SiC	500	UNK[e]	.22	.16	300	930	630	680	u
502	SiC	500	6.1	.26	.24	280	1125	845	715	u
503	SiC	500	5.6	.28	.24	285	1185	900	680	u
504	SiC	1000	4.0	.24[f]	.20[f]	290	950	660	755	96%
505	SiC	1000	4.2	.26	.23	280	910	630	770	89%
506	SiC	500	7.1	.28[g]	.23[g]	335	1015	680	505	100%
507	SiC	500	7.2	.27[g]	.22[g]	295	1045	750	680	100%
508	SiC	500	4.9	.31[h]	.31[h]	280	1040	760	1000[i]	99%
509	SiC	500	6.9	.24[j]	.19[j]	300	1095	795	1005[i]	97%
510	SiC	1000	4.3	.27	.25	295	960	665	985[i]	97%
511	SiC	500	4.3[k]	.27	.23	290	960	670	950	u
512	SiC	500	6.6	.27	.21	290	1080	790	1025[i]	u
513	SiC	1000	4.9	.26	.23	290	960	670	980[i]	u
514	SiC	500[m]	7.4	.24[n]	.19[n]	310	575	265	630[p]	95%[q]
514A	SiC	500[r]	7.8	.23[n]	.18[n]	295	550	255	650[p]	95%[q]

Table 2., continued

Test (#)	Mat'l	Size (μm)	Flow (kg/min)	Total Flux No Flow[a] (MW/sq. m.)	Total Flux Full Flow (MW/sq. m.)	Temperatures Particle Init (K)	Particle Final (K)	Particle Change (K)	Wall (K)	% Lamps ON
515	SiC	1000	2.3	.25	.24	290	945	655	1045	97%
516	SiC	500[s]	8.1	.25	.19	280	965	685	965	96%
517	Silica	1000	6.7	.25	.23	290	740	450	1015	95%
518	SiC	500[s]	7.6	.39	.31	290	1160	870	1185	94%
519	SiC	500[s]	7.6	.42	.35	290	1210	920	1225	92%
520	SiC	500[s]	7.5	.50	.42	285	1305	1020	1460	88%
601	SiC	500	6.1	.00	.00	625	425	-200	N/A	N/A
602	SiC	500	6.1	.00	.00	485	360	-125	N/A	N/A
603	SiC	500	7.2	.00	.00	485	400	-85	N/A	N/A
701	Silica	300	8.5	.24[j]	.18[j]	285	880	595	940	97%
702	Silica	300	6.9	.28[j]	.21[j]	295	960	665	985	97%
703	Silica	1000	5.7	.25	.23	320	725	405	920	u
704	Silica	1000	5.4	.24	.23	330	735	405	925	u
705	Silica	1000	6.7	.26[j]	.24[j]	280	730	450	900	u
706	Silica	1000	4.6	.27	.26	300	785	485	980	
801	SiC	500	13.8[t]	.26	.17	275	990	715	850	98%
802	SiC	500	7.1[t]	.27	.21	285	1075	790	1000	u

NOTE: Values shown here were chosen by noting the time during the test run that the temperature in the catch bin reached its highest value, and retrieving all the other values at that time. Exceptions noted below.

a - Average value of four gages, after flow.
b - Thermocouple #17 unless otherwise noted.
c - Not all sensors connected, estimates.
d - Data suspect, high load cell temp.
e - No data avalable from load cell #3.
f - Only two flux gages with good data.
g - One gage installed, HF3 at rear wall.
h - One gage installed, HF3 at front.
i - Thermocouples changed relative response.
u - values not recorded
j - Average of three gages only.
k - Flow out of hopper obstructed.
m - Mixed size distribution.
n - Only top two sections irradiated.
p - Thermocouple #11.
q - For top two sections only.
r - Better distribution than 514.
s - New batch of 500 μm, SiC.
t - New orifice plate in hopper.

500 μm particles. In general, less than ten percent of the particles were lost in any given run due to convection currents, gaps or access holes in the chute, and prevailing winds. There was no significant change in particle size distributions as a result of multiple passes through the apparatus.

Particle Velocity

The velocity profiles in the vertical direction for silica sand and silicon carbide in the presence of a 0.25 MW/m^2 radiant flux are shown in Figure 10. The smaller silicon carbide particles show a remarkable decrease in velocity after four meters of fall. Unfortunately, no data was obtained for distances beyond 6.66 m, but the velocity was assumed to remain constant for calculating residence times. The velocity decrease is assumed to be due to convective air currents generated within

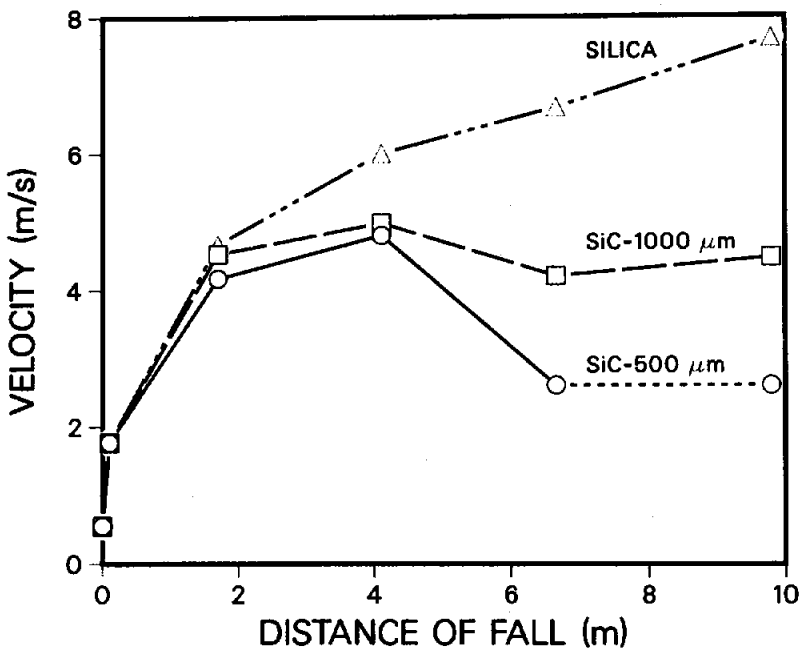

Figure 10. Particle Velocity Profile in Chute with 0.25 MW/m^2 Flux

the chute primarily by the hot particles (not the chute walls). If the convective currents were due to the walls, the velocity changes for the silicon carbide and silica sand particles would be the same because the wall temperatures were equal. Further analysis of the data reveals that the particles above three meters are not influenced by convection currents, indicating the air must have been cooled by transfer of energy to incoming cooler particles and decelerated by the time it reaches the upper part of the chute.

On several test runs, attempts were made to observe the rate of air flow into the chute at the bottom. This flow was barely detectable and was estimated to have a velocity less than 1 m/s. The same type of observation was attempted at the top, with the same result. Since the heated particles are traveling 5 m/s slower than the unheated particles near the center of the chute, it is assumed that the incoming air is heated and accelerated in the lower portion of the chute, then cooled and decelerated as it travels up the chute. The effect of these velocity profiles will be discussed in the next section.

The residence times of the hot particles as a function of position in the chute are shown in Figure 11. A comparison of residence times and velocities for hot and cold particles is shown in Table 3.

Velocity measurements in the 600 series tests revealed an increase in velocity for 500 μm silicon carbide particles at 1.70 m and a decrease at 4.11 m. These particles were preheated to 483 K before being dropped into the chute. In another test, the particles were preheated to 623 K and the velocity measurement at 1.70 m was within 0.02 m/s of the velocity for the 483 K particles. This apparent contradiction with the radiant flux velocity profiles can be explained by heat transfer to the air just sufficient to reduce the dynamic air viscosity and particle buoyancy, but not sufficient enough to generate significant convection currents to oppose the particle motion. The slight decrease in velocity at 4.11 m compared to cold flow data is further evidence that the convection currents were generated by the particles and not the chute walls because there were no hot walls to create the convection currents. These results are summarized in Table 4.

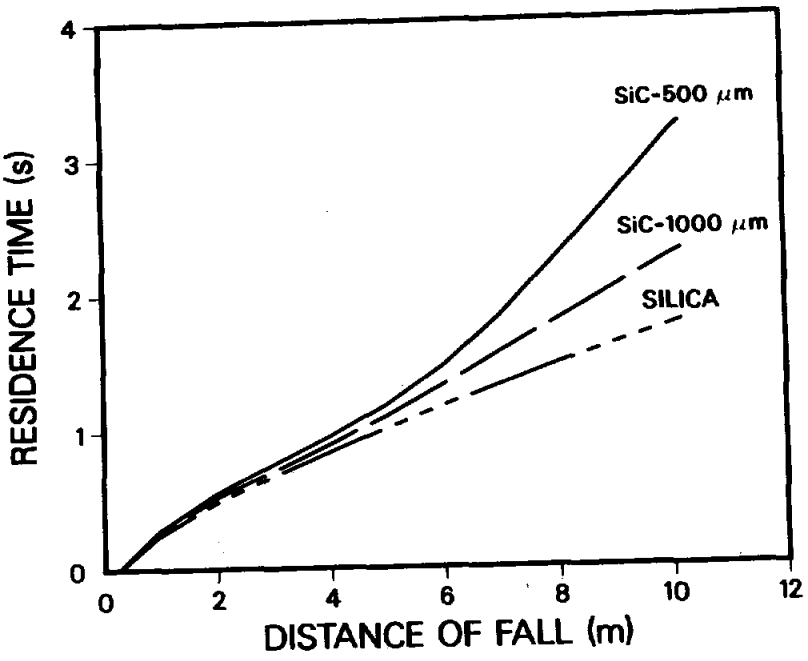

Figure 11. Particle Residence Time in Chute with 0.25 MW/m^2 Flux

Particle Temperature

(a) Final Particle Temperature

Bulk final particle temperature was measured in a catch bin under the chute (see Figure 1). Final particle temperature trends are shown in Figure 12. The effects of absorptivity, particle size, and flux level can be observed.

The effects of absorptivity are apparent by noting the difference in final temperature for silica sand and silicon carbide particles. Measurements made on both materials indicate infrared absorptivities of 0.62 and 0.84 respectively (Appendix A). Because the silicon carbide particles reached higher final temperatures, the

Table 3. Particle Residence Time Data Summary

Cold Flow Data

Velocities (m/s) at Distance Below Discharge Hopper

Mat'l	*Size* (μm)	0.10m	1.70m	4.11m	6.66m	9.80m	Residence Time (s)
SiC	500	1.77	4.92	6.91	7.48	8.59	1.75
SiC	1000	1.77	5.35	7.46	8.52	8.85	1.62
Sand	300	1.77[1]	–[2]	–	–	–	–
Sand	1000	1.77[3]	5.45	6.36	8.37	8.97	1.68

Flux - 0.25 MW/m^2

Velocities (m/s) at Distance Below Discharge Hopper

Mat'l	*Size* (μm)	0.10m	1.70m	4.11m	6.66m	9.80m	Residence Time (s)
SiC	500	1.77[4]	4.17	4.80	2.60	–	3.23
SiC	1000	1.77[4]	4.53	4.98	4.20	4.47	2.29
Sand	300	1.77[4]	–[2]	–	–	–	–
Sand	1000	1.77[4]	4.67	6.00	6.67	7.68	1.77

Residence times were calculated assuming that the particles entered the chute after falling 0.25 m and left the chute after 10.2 m

1. LDV measurements were attempted but not possible, value for 500 μm SiC used.
2. LDV system never functioned for 300 μm silica sand.
3. LDV measurements not attempted, value for 1000 μm SiC used.
4. LDV measurements not attempted, values for cold flow used.

Table 4. Preheated Particle Velocity

	Initial Particle Temperature	
SiC - 500 μm	483 K	623 K
Velocity at 1.70 m	5.16	5.14
Velocity at 4.11 m	6.83	–

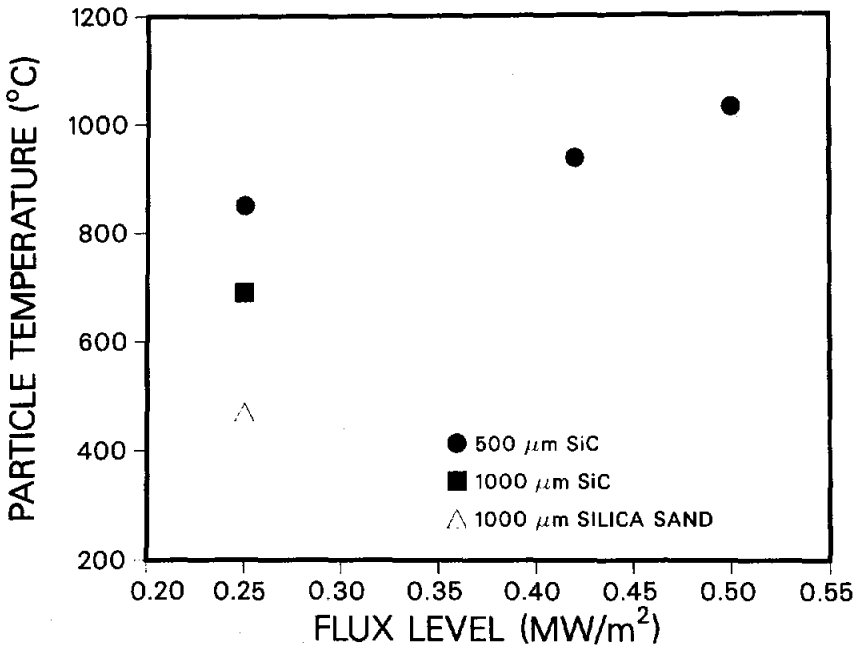

Figure 12. Final Particle Temperature as a Function of Absorptivity, Particle Size, and Incident Radiant Flux Level

residence time for the silicon carbide may be longer than for silica sand, thereby compounding the effect of absorptivity differences.

As expected, the final particle temperature decreased with increasing particle size under constant flux, as shown in tests 502 and 513 for silicon carbide particles and in tests 702 and 705 for silica sand. This effect is primarily due to an increase in particle velocity (a decrease in residence time) in the chute for the larger particles. The larger the particle the greater its free-fall velocity and the lower its residence time. The residence time for tests 502 and 513 was determined to be 3.23 seconds and 2.29 seconds respectively.

The final temperature increased with increasing radiant flux as shown in tests 516, 518, 519 and 520. The highest temperature reached was 1305 K in the presence of a flux of 0.50 MW/m^2 for 500 μm silicon carbide with a mass flow rate of 7.5 kg/min. The increase in temperature with incident flux cannot be linear because, if for no other reason, the specific heat of silicon carbide increases with temperature [6]. However, the energy absorbed per unit mass does appear to be nearly linear as shown in Figure 13. (This linear relationship is more clearly seen when the data is adjusted for differences in mass flow rate, as discussed in the next section.)

The final particle temperature varied considerably when examining all the tests, most of the results being predictable in trend. Since the 400 series tests were conducted to examine characteristics of the system, less care was taken to insure accurate measurement. However, it is interesting to note that the final temperature reached 990 K in test 403 with 300 μm silicon carbide and with a low radiant flux of 0.14 MW/m^2. This temperature is much higher than temperatures for 500 μm particles at comparable flux levels due to the longer residence time of the 300 μm particles.

A strong interdependency exists among the parameters measured in this experiment. For this reason it is more difficult to establish individual relationships than was originally anticipated. As an example of the interdependency, consider the influence of wall temperature on particle temperature. As the flux is increased, both the wall and particle temperatures increase. Therefore, it is not immediately

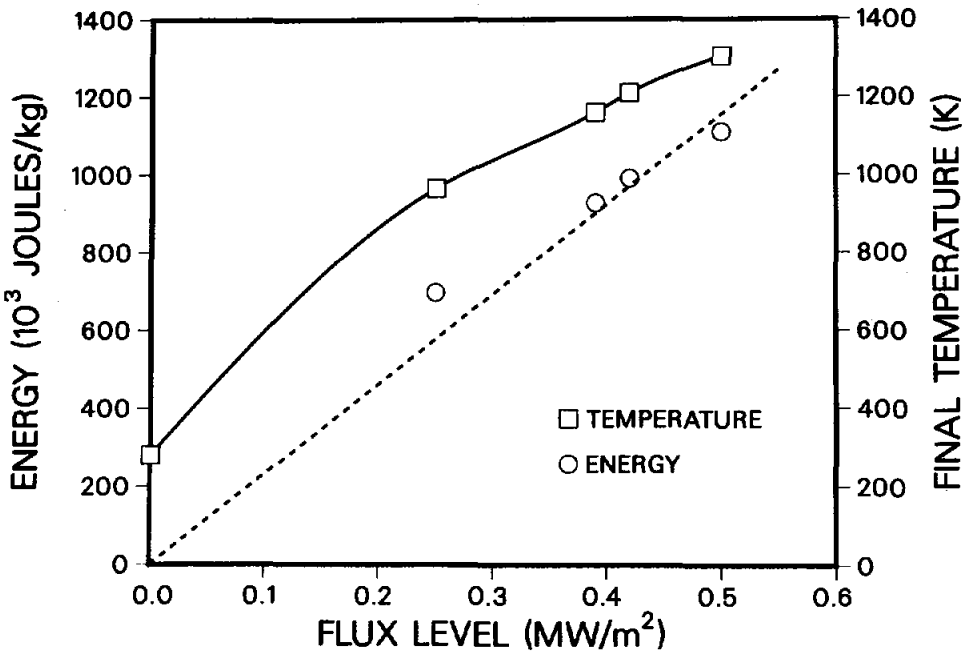

Figure 13. Energy Absorbed per unit mass as a Function of Radiant Flux for 500 μm particles

obvious how to compare final particle temperatures as a function of flux level alone, since the wall temperature played a role in determining final particle temperature. Other examples of interdependency include the simultaneous change in velocity and volume fraction of the particles as flow rate changes.

In addition, the level of incident radiant flux is sensitive to the number of functioning lamps which would periodically burn out. Therefore, repeatability of each test is not exact. Despite these problems, when the appropriate adjustments for comparison of data are made, a consistent set of data evolves.

(b) In-Situ Particle Temperature

In-situ particle temperatures were measured for 500 and 1000 μm silicon carbide particles and 1000 μm silica sand particles. Particle temperature as a function of fall distance for the silicon carbide and silica sand particles is plotted in Figure 14. The particle temperature is a monotonically increasing function of fall distance.

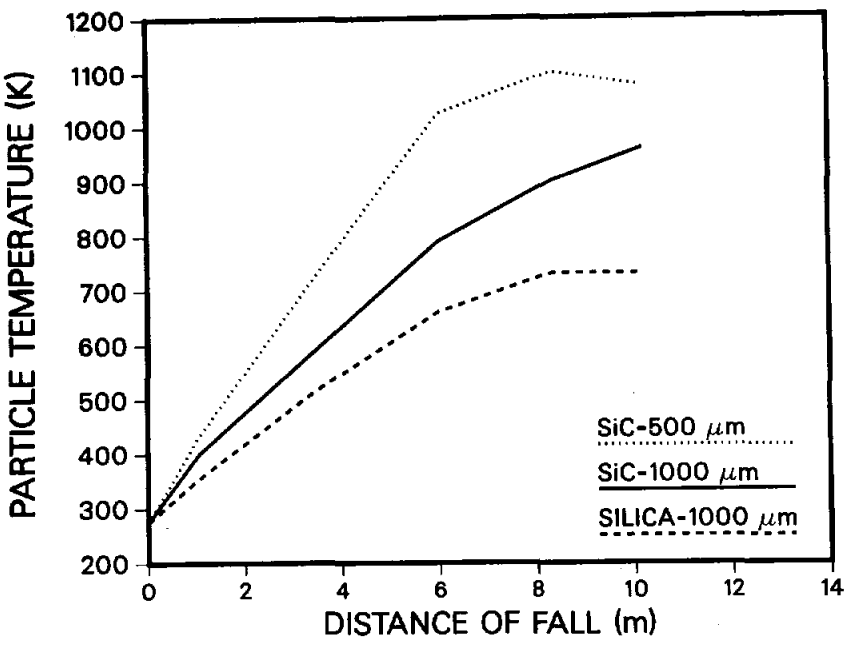

Figure 14. Particle Temperature as a Function of Fall Distance

The temperature increase per unit distance (slope of the curve) decreases as the temperature increases. This decrease is due to the increase in specific heat with increasing temperature. The energy gained between 8.8 m and 10.2 m is small in most cases. This low gain suggests that the final particle temperature measured in the catch bin is probably lower than the actual final particle temperature (as the particle leaves the chute). Radiative and convective energy loss from the particle after it leaves the radiant flux and before its temperature is recorded in the catch bin is most likely responsible for the temperature reading being slightly lower than expected. Therefore, in most cases the temperature measured in the catch bin is a conservative estimate of the particle heating.

In-situ particle temperatures were also measured in the pre-heated, no flux tests (series 600). The particle temperature decrease was non-linear with height, but it was not a quartic function of height (or time) either. This relationship indicates the importance of both convection and radiation in particle heat transfer.

Radiant Flux

Flux measurements made during a test run can be used to calculate the optical depth of the curtain, and indicate net absorption of energy by the particles. These parameters can be deduced from the ratio of heat flux recorded during particle flow to heat flux recorded after particle flow (ratio of transmitted to incident energy, q_p/q). The quantification of optical depth is important because the extinction coefficient for the silicon carbide and silica sand particles is unknown at present. Measurements to determine the extinction coefficient are currently being performed at Battelle Pacific Northwest Laboratories [10].

The use of flux gage measurements to predict optical depth must be approached with caution. Ideally, the measurement of optical depth should be done with a collimated light source and a detector which rejects scattered light [11]. In this case, the detector is larger than the particles and may be detecting scattered energy. Some information can be gained by studying the results nonetheless.

Table 5 indicates the ratio of transmitted to incident energy for test series 450 as a function of distance. (Heat flux measurements were made at the back wall of the chute for all tests in Figure 5.) All other ratios can be obtained from Table 2. The optical depth of the curtain, βL, can be described by

$$-\beta L = ln(q_p/q)$$

where:

$\beta =$ extinction coefficient

$L =$ depth of curtain

$q_p =$ heat flux recorded during particle flow

$q =$ heat flux recorded without particle flow

The calculation to determine optical depth of the particle curtain is most accurately done with measurements taken on the top chute section because only absorption and scattering (not emission) should affect the heat flux recorded at the back wall.

The net absorption of energy by a particle can be surmised from the ratio q_p/q.

Table 5. Ratio of Heat Fluxes During and After Particle Flow as a Function of Fall Distance

Test	1.52 m	3.96 m	6.40 m	8.84 m
451	0.61	0.77	0.89	0.96
452	0.69	0.79	0.84	0.90
453	0.68	0.78	0.83	0.87
454	0.72	0.71	0.81	0.75
502	0.91	0.93	0.90	0.92
503	0.81	0.80	0.87	0.94
505	0.89	0.85	0.90	0.84
509	0.70	0.74	0.94	0.98
510	0.88	0.88	0.97	0.96

As seen in Table 5, q_p/q increases with fall distance. This increase implies that net energy absorption by the particles decreases as fall distance (and particle temperature) increases. This decrease is due to the re-radiative energy loss increasing as the particle temperature rises.

The heat flux gage in the third chute section (at a height of 6.66 m) was traversed in the particle flow to detect any difference in heat flux reading from the front to the back of the chute during particle flow. The results from these tests indicate a negligible change from the middle of the chute to the rear of the chute in absolute flux measurements. However, the flux measurement during particle flow is higher in the center of the chute than in the back, as expected. The absolute flux measurement in the front of the chute was higher than the measurement at the rear wall. This trend is the same as seen in the spatial flux mapping, and indicates that the presence of particles does not affect the spatial flux data measured in the absence of particle flow. The attenuation of flux during particle flow in the front of the chute was also less since there were few particles in front of the gage. This information is summarized in Table 6.

Table 6. Ratio of Heat Fluxes During and After Particle Flow as a Function of Depth in Chute at an Elevation of 6.66 m

Test	Position	Ratio
508	Front	0.93
509	Middle	0.90
507	Back	0.81

ENERGY ABSORPTION AND SYSTEM EFFICIENCY

Consider a very simple model of the system where the chute is essentially a heat exchanger, the lamps a source of heat and the particles the heat transfer media. Assume the particles and the walls are at the same temperature (this is a good assumption in the lower part of the chute), the convective loss by hot particles in the bottom section of the chute is mostly offset by convective heat transfer gain to the cold particles in the top section of the chute, and the re-emitted energy loss from the particles is negligible. The energy absorbed by a single particle is then due to the incident lamp flux and can be expressed as

$$E_a = q\alpha A_p t_r$$

where:

$E_a =$ energy absorbed
$q =$ heat flux seen by the particle
$\alpha =$ absorptivity of the particle
$A_p =$ particle surface area available for absorption
$t_r =$ residence time of the particle in the chute

If a mass of particles is falling through the chute over a period of time t, the energy input to the system over that period is

$$E_{in} = qA_c t$$

where:

E_{in} = energy input to system over time t
A_c = frontal area of the chute admitting the flux
t = total duration of particle flow

Then if n is defined as the particle (number) flow rate, the efficiency of heat collection by the particles can be expressed by

$$Eff = \frac{(q\alpha A_p t_r)nt}{qA_c t}$$

Since a particle towards the rear of the chute is masked from the flux by particles in front, the heat flux is not uniform on all the particles. This effect is compounded because the refractory walls are highly reflective and hence the particles are irradiated from three directions with reflected energy. This variance will be expressed as an effective surface area, $A_p = K4\pi r^2$ where $0 < K < 1$. With this definition of A_p, flux variations from different directions can be accommodated in the constant K. Now the efficiency equation can be written

$$Eff = K'\alpha r^2 t_r n$$

where:
K' = $\frac{K4\pi}{A_c}$
r = particle radius

Therefore, for any given system the efficiency increases linearly with absorptivity, residence time, and particle flow rate, and increases as the square of the particle radius, assuming no change in heat flux to the particles. (The radius and particle flow rate are often related.) For a given energy input, the energy absorbed varies in precisely the same manner as the efficiency. It is important to note that the five terms in this model are not necessarily dependent. They can be dependent, but conditions can be generated that allow each to vary independently of the other. For example, residence times can be varied independently of particle radius by varying the initial particle velocity.

In this experiment, r^2n is constant for test series 450, 500, 600 and 700 since the same slit opening in the bottom of the discharge hopper was used to introduce the particles into the chute. As the particle radius increases, the number of particles that can be in the slit at any instant of time decreases according to the particle cross sectional area. The same argument holds for the heat flux variation in the chute from test to test, which implies that the efficiency varies only with absorptivity and residence time. Figure 15 demonstrates this effect by comparing the energy absorbed per unit mass and the residence time for several tests using similar radiant flux levels. Specific heat values for this figure were obtained from Reference [6]. Since all the tests were conducted at the same lamp voltage, the data were divided by the fraction of lamps functioning rather than adjusted according to flux gage readings. Also, only tests where velocity data were taken at 6.66 m and 9.8 m were used, to give confidence in residence time data.

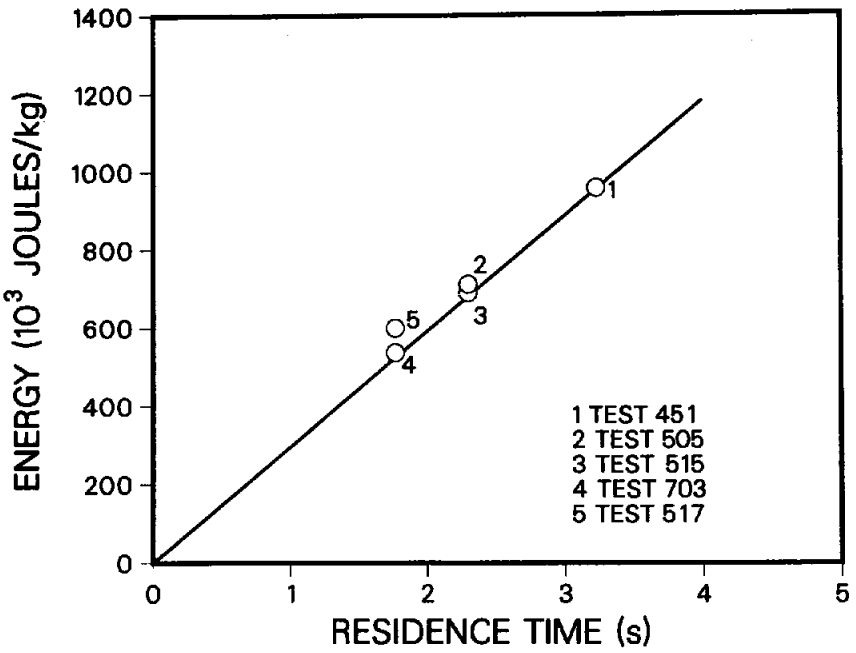

Figure 15. Energy Absorbed per unit mass as a Function of Particle Residence Time

Also shown in Figure 15 are the results from two silica sand tests adjusted for differences in absorptance. These data fall somewhat above the linear relationship, but that may be explained by a change in the heat flux profile through the depth of the chute as a result of lower particle absorptance, and significant differences between particle temperature and wall temperature resulting in an additional heat flux to the particles. The increase in heat to the particles from the walls will result in a larger temperature increase for the same increase in flux level, and therefore yield a higher efficiency.

Based on the model, energy absorbed as a function of flux level (Figure 13) can be replotted adjusting the values according to the mass flow. Figure 16 shows the adjusted data and indeed the values fit a linear relationship very well. The data points at lower flux levels are expected to diverge from this relationship, since as

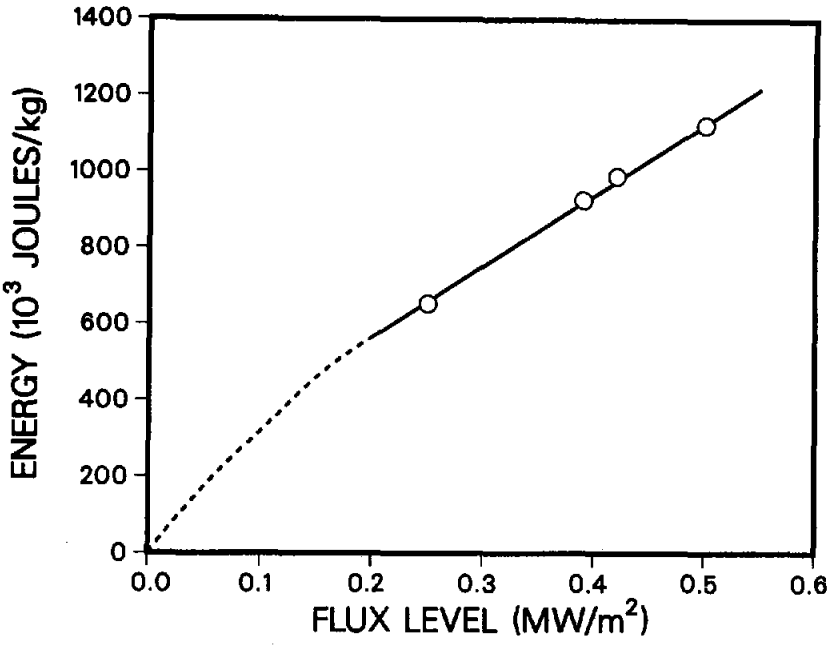

Figure 16. Energy Absorbed (adjusted) per unit mass as a Function of Radiant Flux

before, heat transfer from the walls to the particles will play a role in the lower particle temperature regime. The dotted line on Figure 16 is a prediction of what would happen at lower flux levels (values were not measured).

Table 7 indicates efficiencies for many of the tests summarized in Table 2. Some important trends can be deduced from this table. A trend which can be seen from the results of tests 513 and 515, and tests 801 and 802 is that efficiency increases with mass flow rate. However, the final particle temperature also decreases with mass flow rate (see Table 2). Therefore, efficiency and final particle temperature cannot be increased simultaneously. This compromise between final particle temperature and mass flow rate to obtain increased efficiency is important for receiver design considerations.

Another important result is that efficiency decreases as heat flux is increased. This decrease can be seen in tests 516, 518, 519, and 520 and is a result of the effective absorption surface area decreasing. This effective area decreases because the re-radiative losses from the particles increases with increasing temperature, reducing the net energy absorption.

ENERGY BALANCE

An energy balance can be performed on the system as shown below:

$$E_{in} = E_{abs,p} + E_{abs,w} + E_{radloss} + E_{conv} + E_{cond}$$

where:

E_{in} = energy which enters the chute
$E_{abs,p}$ = energy absorbed by the particles
$E_{abs,w}$ = energy absorbed by the walls
$E_{radloss}$ = radiative energy loss
E_{conv} = convective energy loss
E_{cond} = conductive energy loss through the chute wall

Table 7 - Efficiency of Energy Collection

Test Number	*Material*	*Size* (μm)	*Flow* (kg/min)	*Flux* (MW/m^2)	*Efficiency** (*percent*)
405	*SiC*	500	14.0	0.10	27.4
406	*SiC*	500	12.1	0.21	19.0
407	*SiC*	500	7.2	0.28	12.9
451	*SiC*	500	6.7	0.29	11.9
452	*SiC*	500	6.5	0.27	12.0
453	*SiC*	500	7.2	0.25	13.9
502	*SiC*	500	6.1	0.26	11.6
503	*SiC*	500	5.6	0.28	10.7
505	*SiC*	1000	4.2	0.26	5.6
506	*SiC*	500	7.1	0.28	10.6
507	*SiC*	500	7.2	0.27	11.7
510	*SiC*	1000	4.3	0.27	6.1
512	*SiC*	500	6.6	0.27	11.3
513	*SiC*	1000	4.9	0.26	7.2
515	*SiC*	1000	2.3	0.25	3.4
516	*SiC*	500	8.1	0.25	12.5
517	*Silica*	1000	6.7	0.25	6.6
518	*SiC*	500	7.6	0.39	10.1
519	*SiC*	500	7.6	0.42	10.0
520	*SiC*	500	7.5	0.50	9.2
703	*Silica*	1000	5.7	0.25	5.4
704	*Silica*	1000	5.4	0.25	5.5
706	*Silica*	1000	4.6	0.27	4.7
801	*SiC*	500	13.8	0.26	21.3
802	*SiC*	500	7.1	0.27	12.1

* The efficiencies for this test are drastically lower than efficiencies expected for a cavity solid particle central receiver. The reason for the low efficiencies in this experiment is due primarily to the aperture size. The area of the aperture is one third the total chute area. In an actual solid particle cavity receiver, the ratio of aperture area to cavity area would be less than 0.1 [9].

Four of the six terms in this equation can be calculated directly from measurements taken during each test. The two terms which are more difficult to quantify are $E_{radloss}$ and E_{conv}. These two terms cannot be deduced from measured quantities. As mentioned earlier, the air flow at the top and bottom of the chute was observed and did not appear to be significant. However, no specific air flow measurements

were conducted. Based on these observations, it is believed that convective losses were minimal because the energy gained by the air in the lower portion of the chute was transferred to the "cold" particles in the upper portion of the chute.

By calculating the other four terms from measured quantities, the magnitude of the combined radiative and convective loss terms can be deduced. For 450 series tests, the combined radiative and convective losses are approximately 79 percent of the incident energy. Assuming small convective losses implies large radiative losses. This is not surprising considering the geometry of the chute. The ratio of aperture to chute area is very large for this geometry compared to cavity geometries normally considered for central receivers. A calculation using SHAPEFACTOR [7] and RADSOLVER [8] supports the conclusion that radiative losses from the chute are large. (The calculation for radiative losses was done assuming no particles in the chute.) Table 8 provides a sample energy balance performed on Test 451. This test is believed to be representative in this experiment, however; this test is not representative of an actual solid particle receiver. Efficiencies of 70 percent have

Table 8. Representative Test Configuration Energy Balance

Energy Mechanism	Percent of E_{in}
Radiative Loss	72*
Convective Loss	07
Absorbed by Particles	12
Absorbed by Chute	03
Conducted by Chute	06

* The radiative loss in this experiment is drastically larger than expected in a cavity solid particle central receiver. The reason for the high radiative loss in this experiment is due primarily to the aperture size. The area of the aperture is one third the total chute area. In an actual solid particle cavity receiver, the ratio of aperture area to cavity area would be less than 0.1 [9].

been calculated for a 5 MW_t solid particle central receiver sized for the Central Receiver Test Facility (CRTF) [9].

CONCLUSIONS

A major step in proving the technical feasibility of the solid particle receiver concept has been accomplished by heating free-falling particles to temperatures in excess of 1300 K with a moderate radiant flux (0.5 MW/m^2). Particle absorptivity, size, mass flow rate and wall temperature are important parameters in dictating the final particle temperature.

A simple model describing system efficiency has been developed to predict the effect of these parameters on final particle temperature and energy absorbed. The experimental data agree well with the trends predicted by this model. Efficiency was seen to increase linearly with absorptivity, residence time, and the product of particle flow rate and the radius squared. It is often the case that increasing efficiency decreases final particle temperature. This compromise between efficiency and final particle temperature will be important for receiver design considerations. As expected, the effects of radiative emissive loss from the particles was seen as the final particle temperature increased.

Convective currents generated by hot particles heating the surrounding air had a significant impact on particle residence time in the radiant flux. The convective air velocity opposing particle motion increased residence times by as much as a factor of three. Although convective air currents in a cavity will be different from those in the chute geometry used in this experiment, they are important enough to warrant further study. Particle sizes 300 μm and below did not have enough force to overcome the convective velocity in this experiment, indicating size limitations may be imposed on the particles. Nevertheless, the convective currents act in favor of heating particles to high temperatures by increasing residence times.

The data obtained from this experiment verifies that free-falling particles can

be used as the working media in a high temperature solar central receiver. In addition, the experimental data obtained will aid in analytical model verification and receiver design.

APPENDIX A – OPTICAL PROPERTY DATA

Absorptance measurements made on silicon carbide and silica sand particles are shown in this appendix. These measurements were performed at Battelle Pacific Northwest Laboratories on packed particle samples.

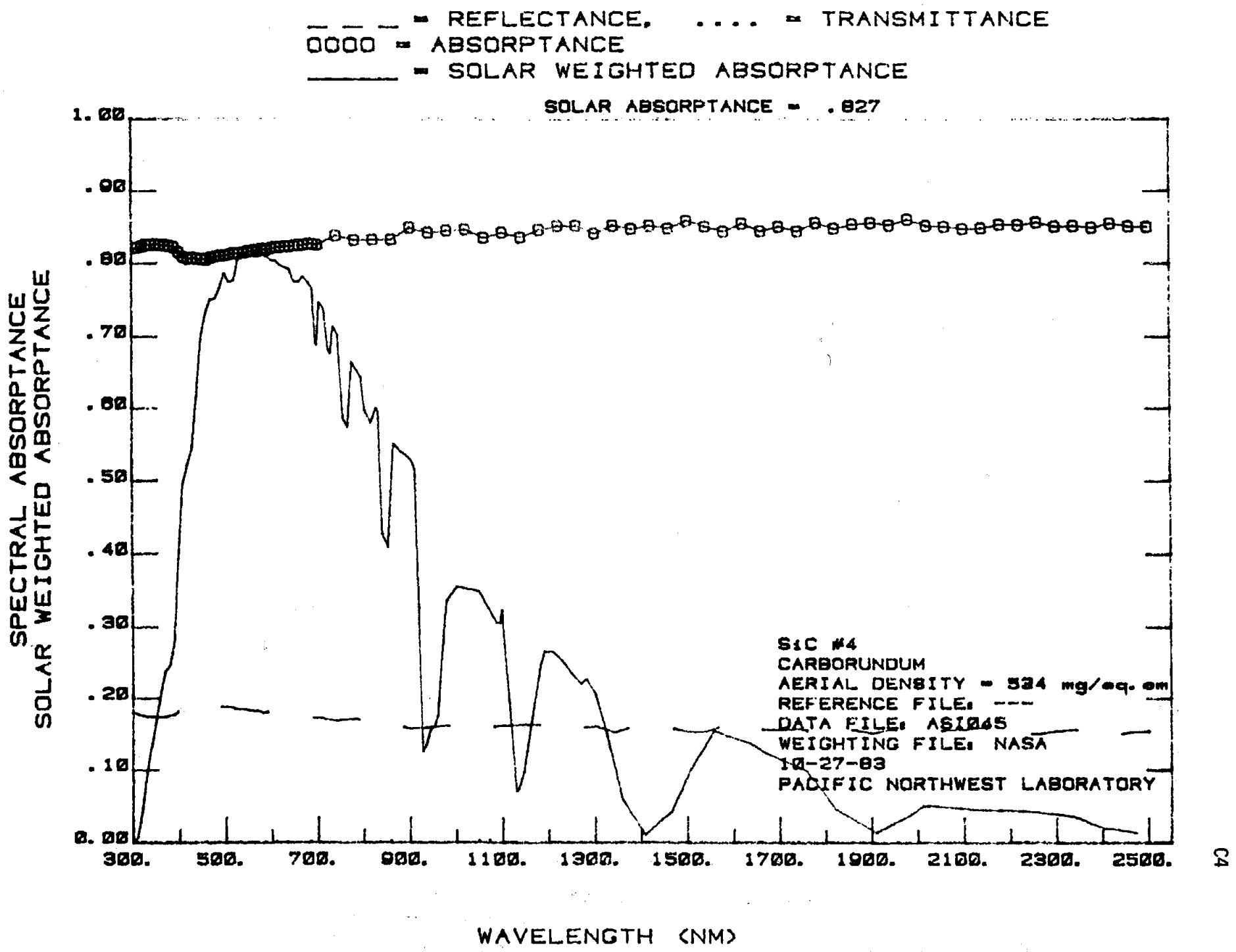
_ _ _ _ = REFLECTANCE, ... = TRANSMITTANCE
0000 = ABSORPTANCE
_____ = SOLAR WEIGHTED ABSORPTANCE
SOLAR ABSORPTANCE = .827
SPECTRAL ABSORPTANCE
SOLAR WEIGHTED ABSORPTANCE
1.00
.90
.80
.70
.60
.50
.40
.30
.20
.10
0.00
300.
500.
700.
900.
1100.
1300.
1500.
1700.
1900.
2100.
2300.
2500.
WAVELENGTH (NM)
SiC #4
CARBORUNDUM
AERIAL DENSITY = 524 mg/sq.cm
REFERENCE FILE: ---
DATA FILE: ASI045
WEIGHTING FILE: NASA
10-27-83
PACIFIC NORTHWEST LABORATORY

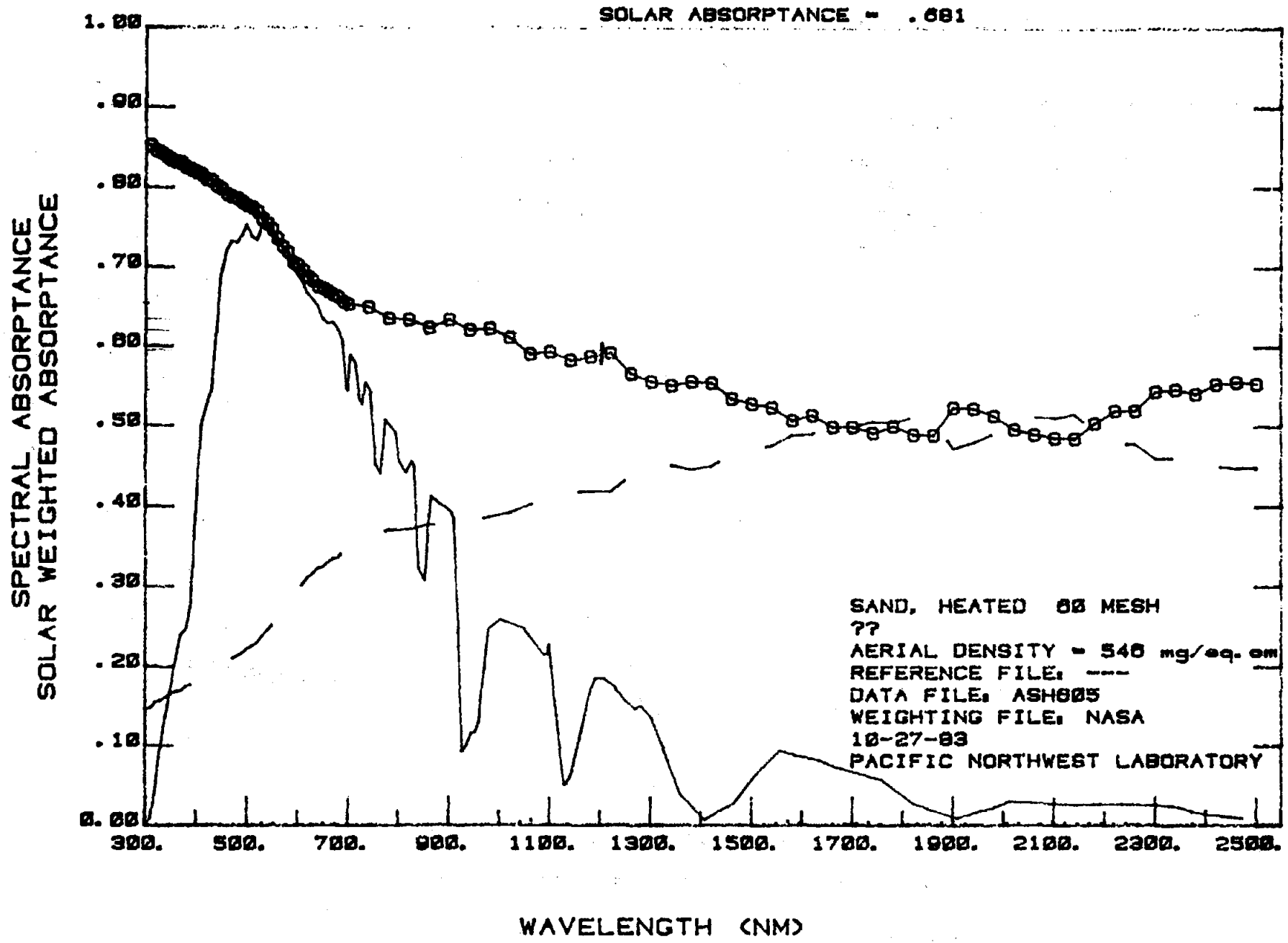
_ _ _ _ = REFLECTANCE, ... = TRANSMITTANCE
0000 = ABSORPTANCE
_____ = SOLAR WEIGHTED ABSORPTANCE
SOLAR ABSORPTANCE = .681
SPECTRAL ABSORPTANCE
SOLAR WEIGHTED ABSORPTANCE
1.00
.90
.80
.70
.60
.50
.40
.30
.20
.10
0.00
300.
500.
700.
900.
1100.
1300.
1500.
1700.
1900.
2100.
2300.
2500.
WAVELENGTH (NM)
SAND, HEATED 80 MESH
??
AERIAL DENSITY = 540 mg/sq. cm
REFERENCE FILE: ---
DATA FILE: ASH005
WEIGHTING FILE: NASA
10-27-83
PACIFIC NORTHWEST LABORATORY

APPENDIX B – SAMPLE DATA OUTPUT

This appendix contains sample data output. Included are plots illustrating radiant heat flux, mass flow, initial particle temperature, final particle temperature, chute temperature, and particle velocity as functions of time. The scale for temperature is always 0 to 1000 °C for consistency.

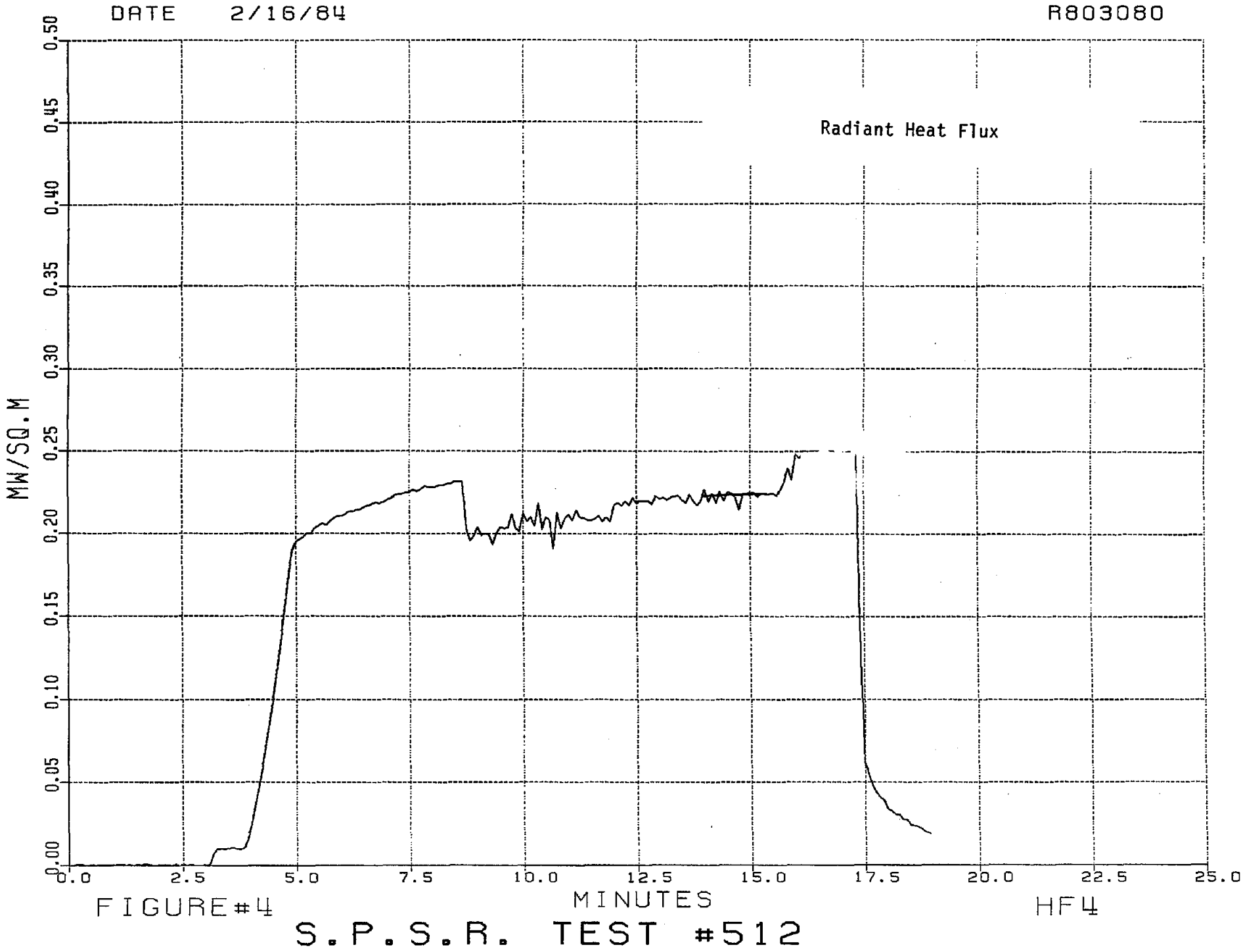

FIGURE#4

S.P.S.R. TEST #512

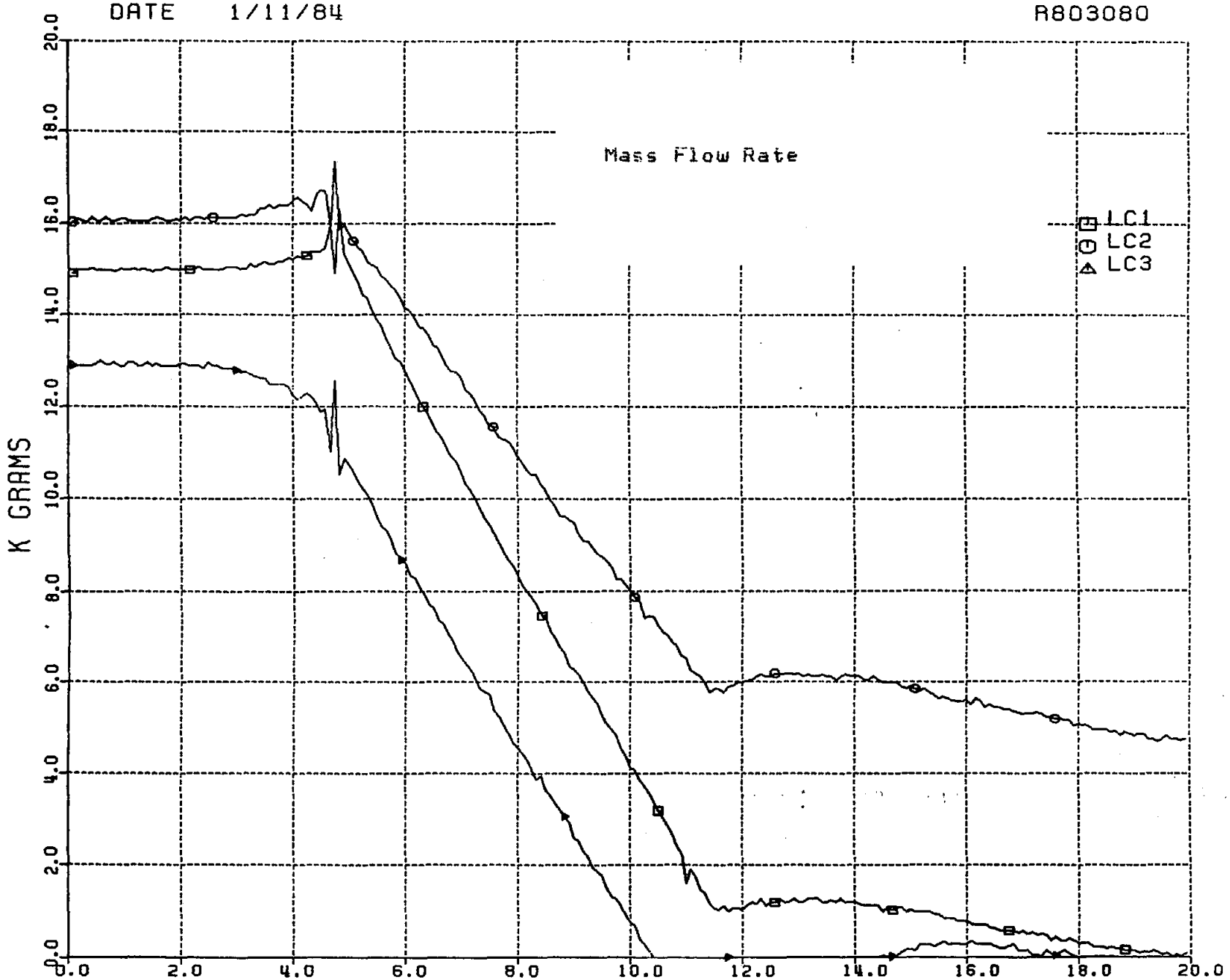

FIGURE#3

S.P.S. REC. TEST #503

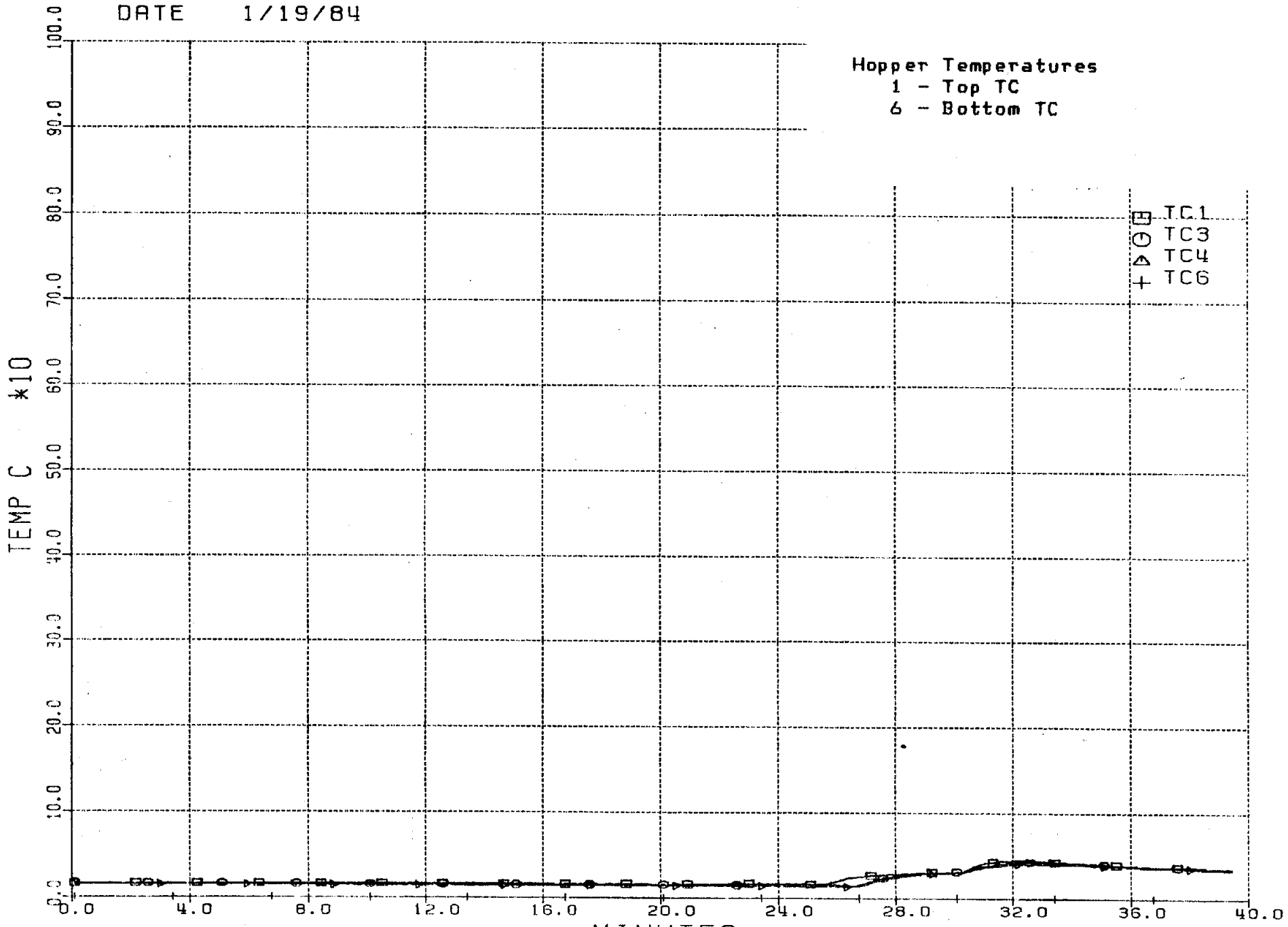

FIGURE #6

S.P.S. REC. TEST #504

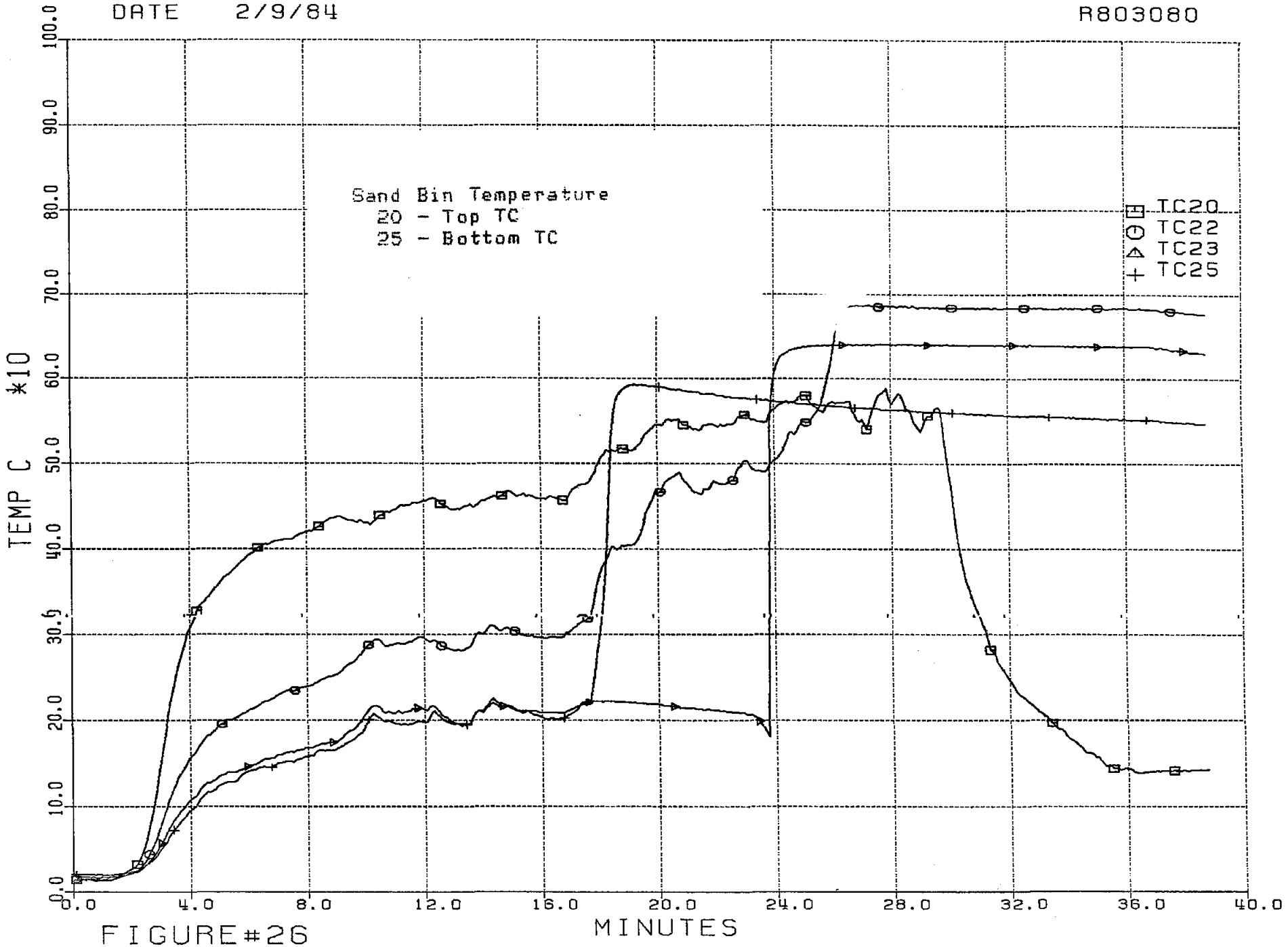

FIGURE#26

S.P.S. REC. TEST #510

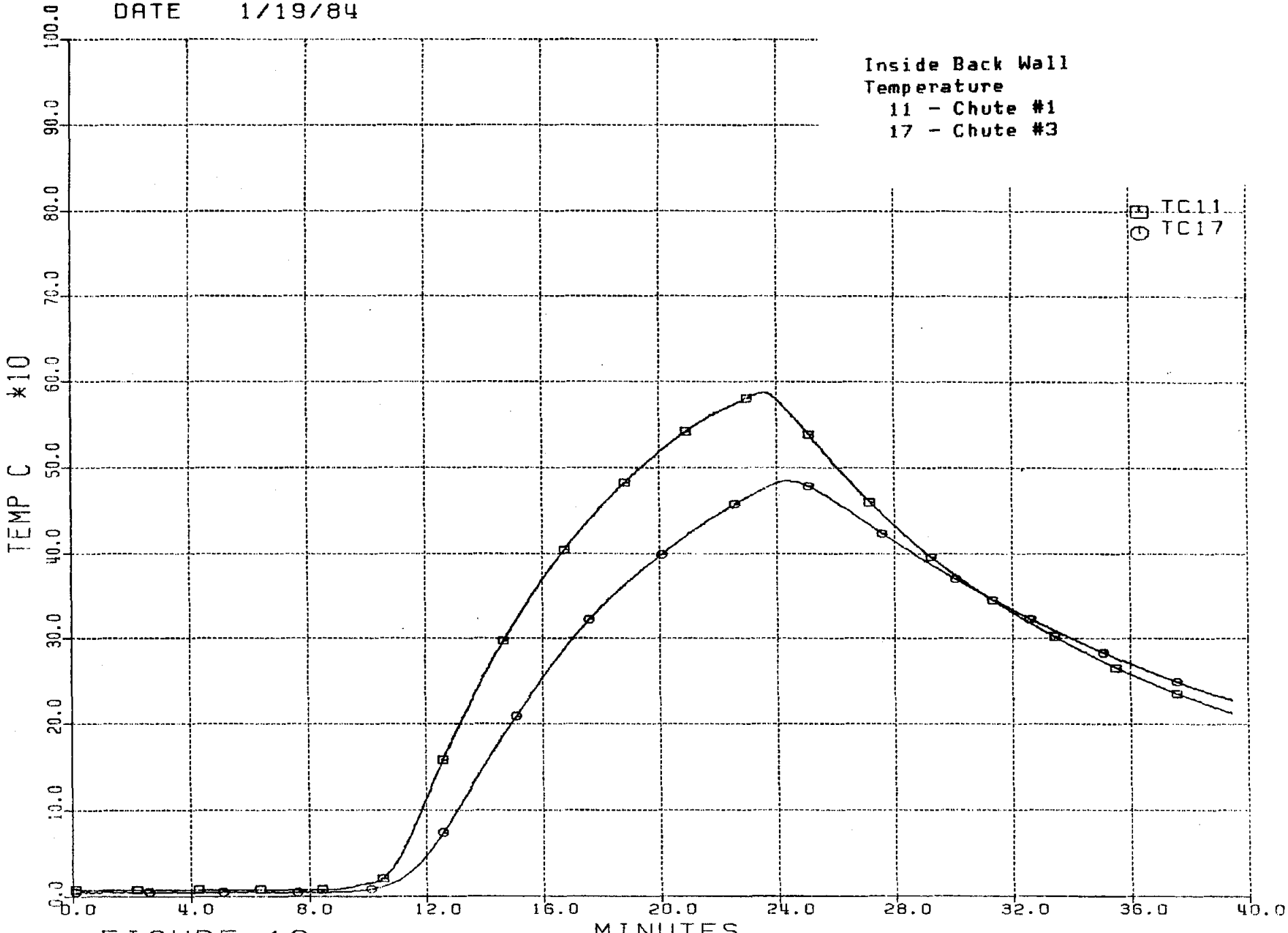

FIGURE#18

S.P.S. REC. TEST #504

Particle Velocity Data

TEST ID: 206

VELO	CYC	VELO	CYC	VELO	CYC	VELO	CYC	VELO	CYC	VELO	CYC	VELO	CYC
7.5	9	7.4	8	6.6	9	7.5	10	7.9	8	5.7	13	8.1	8
7.1	8	7.2	8	8.0	8	7.4	10	7.7	8	8.6	8	7.4	8
6.9	11	7.8	17	7.2	8	7.2	22	7.4	35	8.8	8	8.8	10
8.2	9	7.4	8	6.9	8	8.2	8	5.4	18	8.5	26	8.1	8
7.9	8	7.4	8	7.2	11	7.6	9	7.7	9	6.8	11	7.9	24
7.8	8	8.8	8	7.0	23	8.4	8	7.3	9	7.4	12	5.4	8
7.8	10	8.4	8	6.9	8	7.9	13	7.1	40	7.1	8	7.9	14
6.8	10	8.1	25	7.0	8	7.8	13	7.5	26	7.8	9	5.6	12
6.8	9	7.8	30	7.6	13	7.8	8	8.6	10	8.3	27	7.7	19
5.9	15	7.2	25	7.8	12	7.6	9	7.5	10	7.8	9	7.6	28
.2	9	7.4	10	7.6	16	7.9	9	7.9	9	8.2	12	8.2	15
6.8	8	7.5	8	7.3	10	8.3	16	7.4	11	7.7	15	7.5	10
7.4	18	7.6	16	8.1	12	7.3	10	7.3	15	7.1	8	8.2	11
7.7	21	6.9	12	8.2	34	7.7	21	7.4	12	6.8	12	7.2	30
7.4	28	6.8	8	7.9	12	7.7	22	7.9	16	7.9	8	7.7	8
7.4	11	7.9	13	8.0	13	7.7	13	7.8	20	8.5	20	7.8	10
7.5	8	7.1	13	7.7	10	7.2	20	7.6	8	8.0	11	7.3	16
7.8	9	7.6	18	7.9	15	7.6	9	7.8	16	7.6	22	7.9	32
7.2	15	6.1	9	7.6	28	7.9	11	7.2	17	8.0	12	8.3	12
7.0	15	6.6	65	7.6	9	7.5	8	6.9	17	7.4	13	7.9	15
7.1	16	7.5	22	7.5	14	6.4	19	7.5	16	7.9	10	7.6	10
7.6	12	7.8	9	7.2	13	7.1	12	6.5	10	7.5	11	7.6	42
7.1	13	6.8	8	7.3	9	7.1	14	7.7	9	7.7	9	6.9	8
7.4	24	7.0	25	7.7	12	8.4	17	7.2	10	6.9	37	7.1	14
.5	24	8.1	8	7.9	9	7.6	22	7.7	8	7.4	10	8.6	8
5.8	12	5.6	13	7.2	11	7.8	24	7.4	14	7.6	21	7.9	9
7.9	11	8.4	8	7.4	25	8.2	9	8.2	8	8.4	12	7.4	13
7.2	9	7.3	15	8.1	12	7.4	14	8.0	13	7.7	20	8.0	9
8.3	8	7.5	35	7.7	14	8.4	9	7.2	13	8.1	13	7.4	9
7.4	18	7.9	11	6.7	10	7.6	25	6.8	11	7.1	36	7.6	8
7.5	8	8.0	8	7.7	11	6.1	9	7.3	22	6.5	21	5.6	13
7.4	11	7.2	24	7.3	9	8.0	14	7.6	35	7.5	12	8.6	8
6.8	8	7.5	39	7.3	11	7.8	54	6.9	8	8.9	15	7.7	8
7.2	12	6.2	9	7.7	15	8.2	12	6.9	10	7.5	12	7.6	8
7.4	9	6.8	15	7.4	33	7.0	12	7.3	8	8.1	8	6.7	12
8.1	9	6.4	10	7.0	10	7.7	9	7.4	8	7.6	9	7.5	31
7.0	36	8.1	10	7.6	10	7.6	21	7.0	13	7.4	8	6.9	8
.8	17	6.9	8	7.8	42	6.4	22	8.4	10	7.7	9	7.6	40
6.6	17	7.3	25	7.7	8	7.2	10	7.8	28	6.9	10	7.8	16
7.4	8	7.4	12	7.6	22	7.9	9	7.4	21	8.4	10	6.3	14

MEAN: 7.4784 M/SEC

STANDARD DEVIATION: .6036 M/SEC

TURB. INTENS.: 8.0708

VALID DATA COUNT: 282

CYCLES MEASURED: 8

DATA COUNT REQUESTED: 302

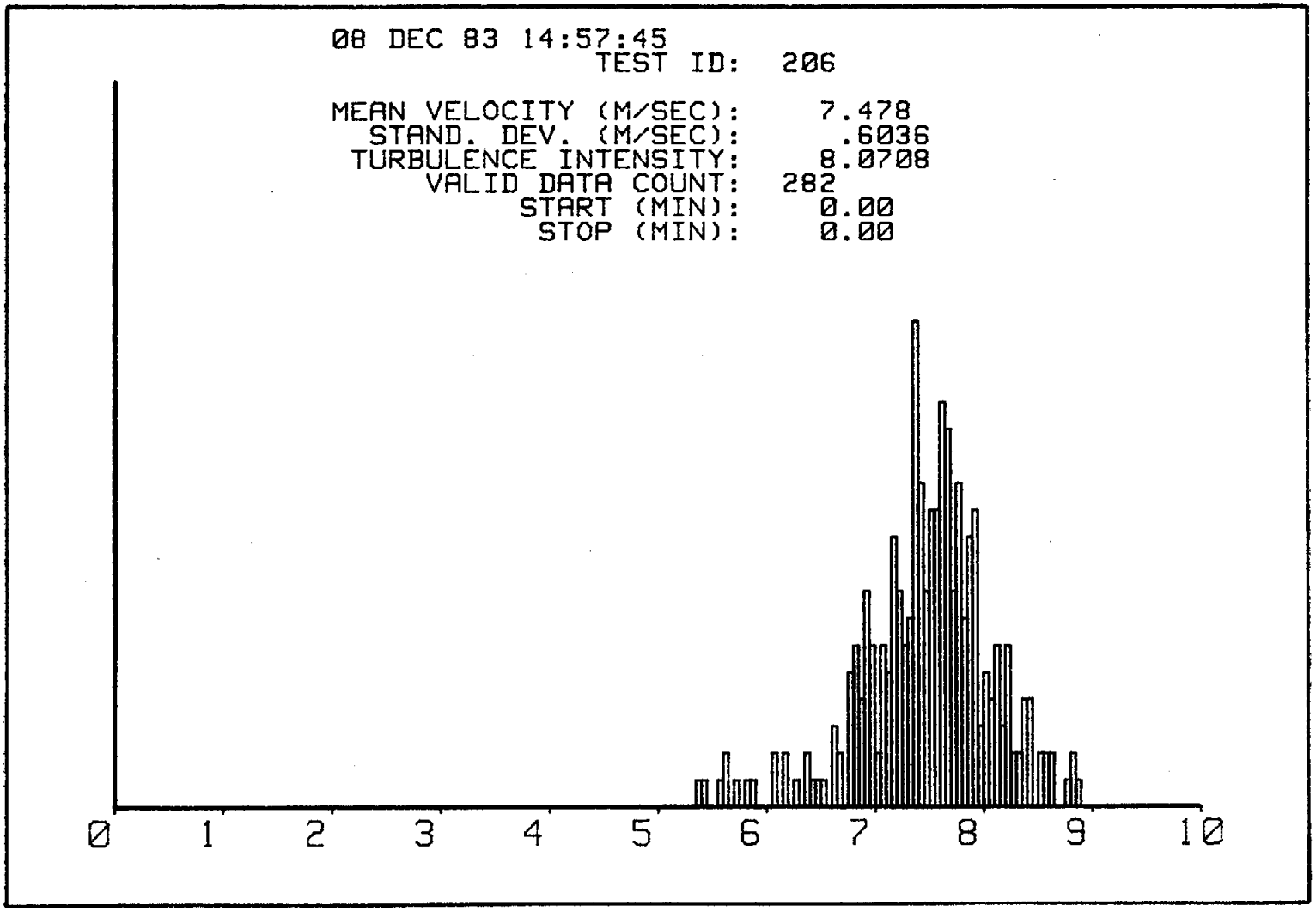

Particle Velocity Histogram

APPENDIX C - SPATIAL FLUX DISTRIBUTION MEASUREMENTS

This appendix contains memorandums from P. L. Class and J. T. Nakos to B. R. Steele detailing spatial flux distribution measurement and results.

Sandia Laboratories

Albuquerque, New Mexico
Livermore, California

date: November 17, 1983

to: B. R. Steele, 8453

from: P. L. Class, 7531

subject: Solid Particle Radiant Heat Test - Flux Distribution Measurements (R803080)

A series of over 100 measurements of heat flux were made within the calibration test chute where the horizontal, vertical and depth position was varied in a systematic manner. The experimental methodology and the results of these measurements are discussed in this memo.

The Experimental Setup

The experimental setup consists of 1) a sheet metal chute (U-shape cross section) approximately 96 inches long by 14 inches wide by 7 inches deep insulated on the inside with 1 inch of Fiberfrax LD refractory insulation board, 2) a heater array assembly consisting of two radiant panels approximately 12 inches wide and 46 1/4 inches high placed vertically one above the other and supported by a frame, 3) a heat flux gage indexing assembly mounted behind the receiver chute, 4) a water-cooled heat flux probe, and 5) a cooling fan and ductwork. The setup is shown in operation in Figure 1. The heat flux probe indexing assembly allows the probe to be accurately positioned in three perpendicular ordinates while maintaining the centerline of the probe perpendicular to the lamp array, as shown in Figure 2. The heat flux probe assembly, shown in Figure 3, consists of a Hycal 1301 series circular foil heat flux transducer mounted in a stainless steel holder that has a series of water passages and ports supplying cooling to both the transducer and itself. Figure 4 shows the heat flux probe installed on the calibration chute within the indexing assembly.

The calibration setup was meant to be representative of the test configuration so that heat flux measurements and distributions derived from the calibration setup could be directly applied to the test configuration. To that end, the same hardware, quartz glass windows, cooling fan and air duct, lamp distribution, and relative position of array to chute were maintained.

Test Procedure

All measurements of flux were made in such a way as to eliminate as much as possible other variables affecting flux measurements other than transducer position. This was accomplished by the following procedure:

1. The radiant heat source (the lamps) were operated at the same voltage for each data position.

2. The heat source was operated until the same temperature conditions were achieved on the inner refractory surface of the chute.

3. The positioning of the probe was consistent with respect to perpendicularity to the heat source.

4. The temperature of the probe was monitored during the tests to ensure the integrity of the heat flux transducer.

5. In the interests of ease of data collection, the probe was fixed in horizontal and vertical position, and measurements were taken at incremented depth locations, allowing sufficient time for about five data scans at each depth position.

Results

The results of the flux measurements for the depth variable are summarized in Figure 5. The differences in flux near the front of the chute from the fan side to the opposite side are probably due to the lack of air deflectors on the opposite side. The differences are about 10%.

The vertical flux measurements are shown in Figure 6. The position related variations are due to some of the spectral effects of the aluminum reflector and the partial blockage of the lamp envelopes to the reflected energy. This effect is lessened as the transducer moves into the chute, where it sees more of the reradiated energy from the side walls of the chute.

The horizontal variations in flux measurements, shown in Figure 7, indicate a flux uniformity in the measurements across the chute from the mid-depth position (3" back) to the rear wall position (6" back). The front chute measurements show the typical distribution one would calculate using view factor geometry. The presence of the air deflectors on both sides of the chute and their contribution to reradiation increases the symmetry about the center of the chute as compared to the data in Figure 5.

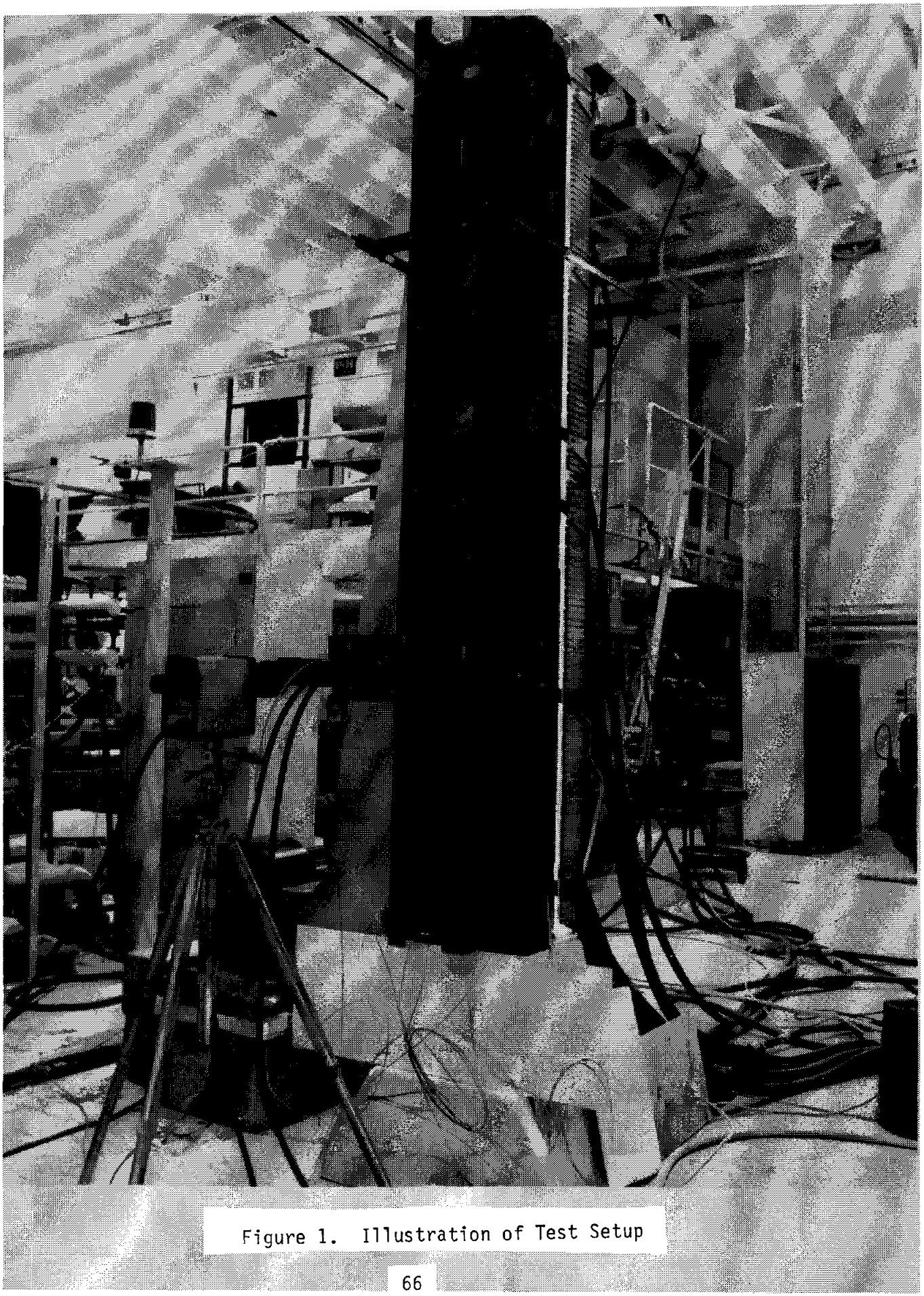

Figure 1. Illustration of Test Setup

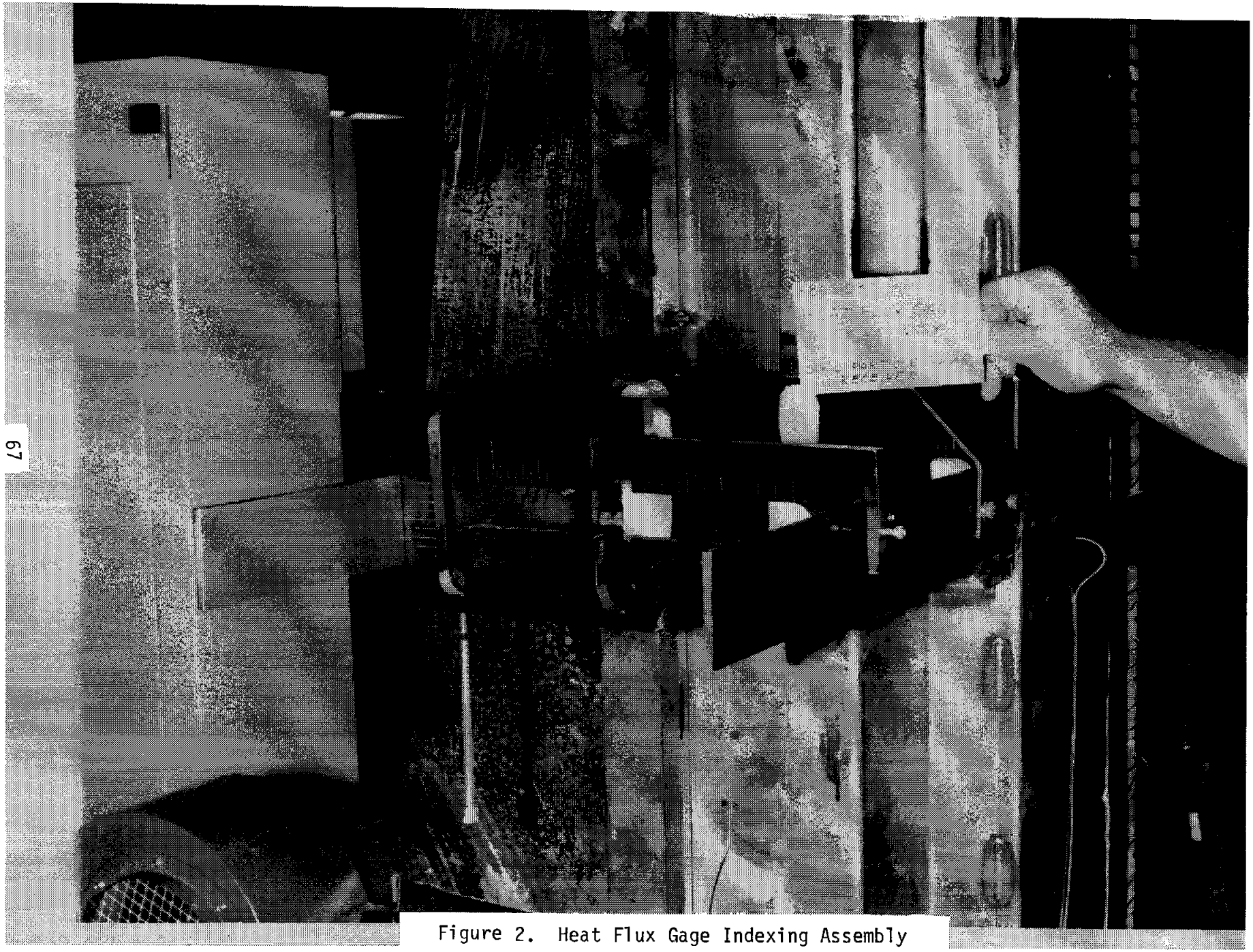

Figure 2. Heat Flux Gage Indexing Assembly

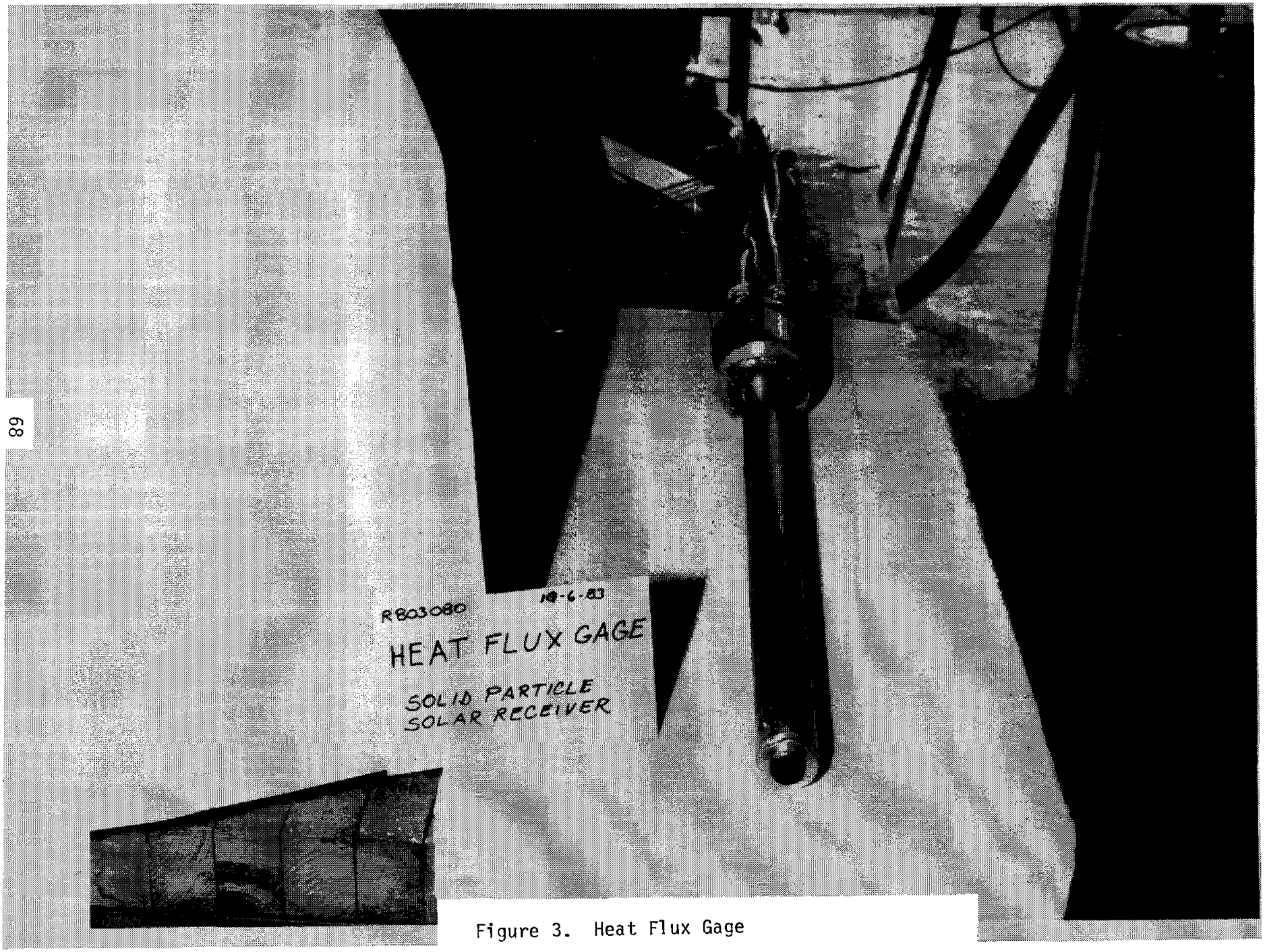

Figure 3. Heat Flux Gage

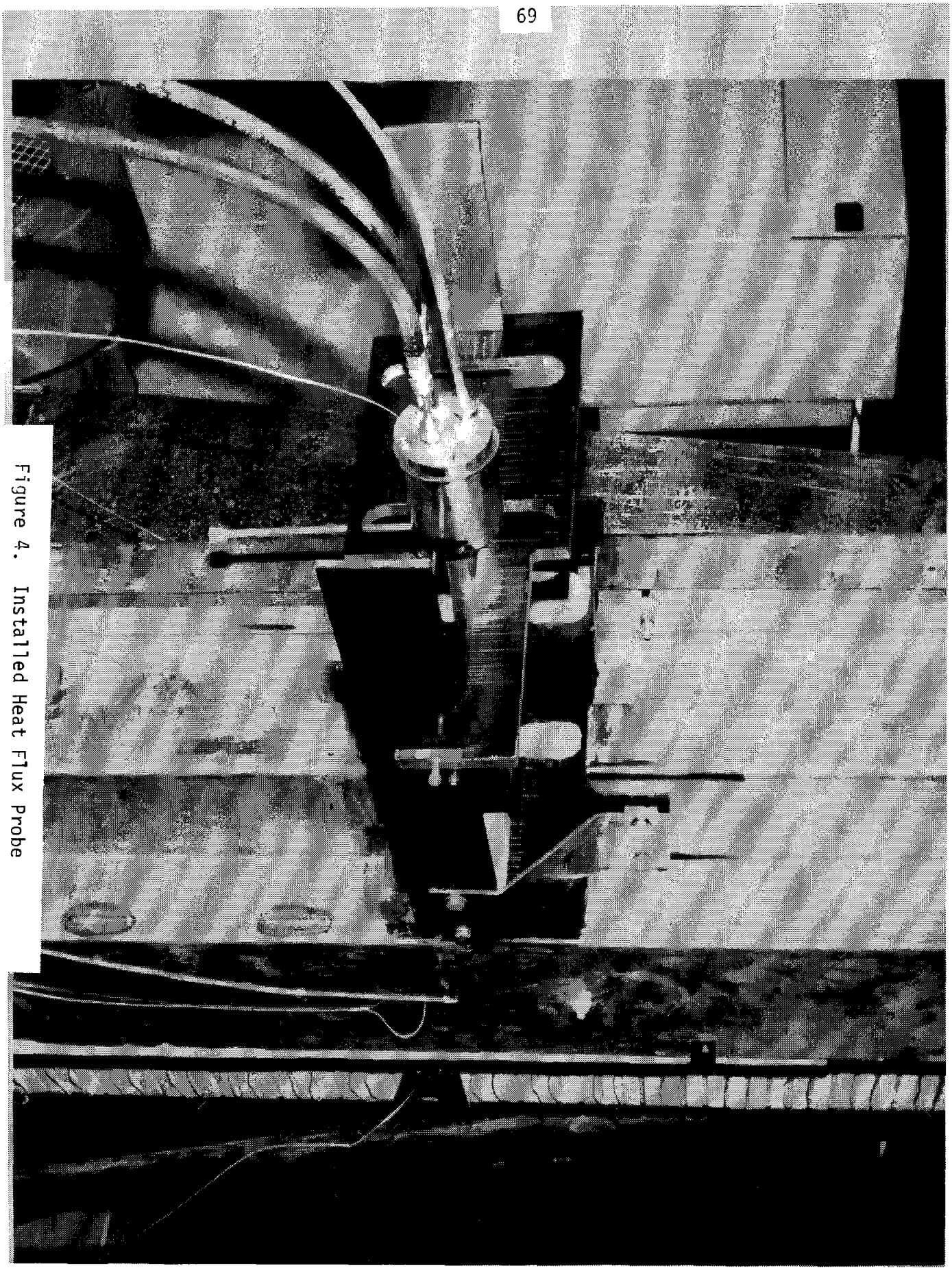

Figure 4. Installed Heat Flux Probe

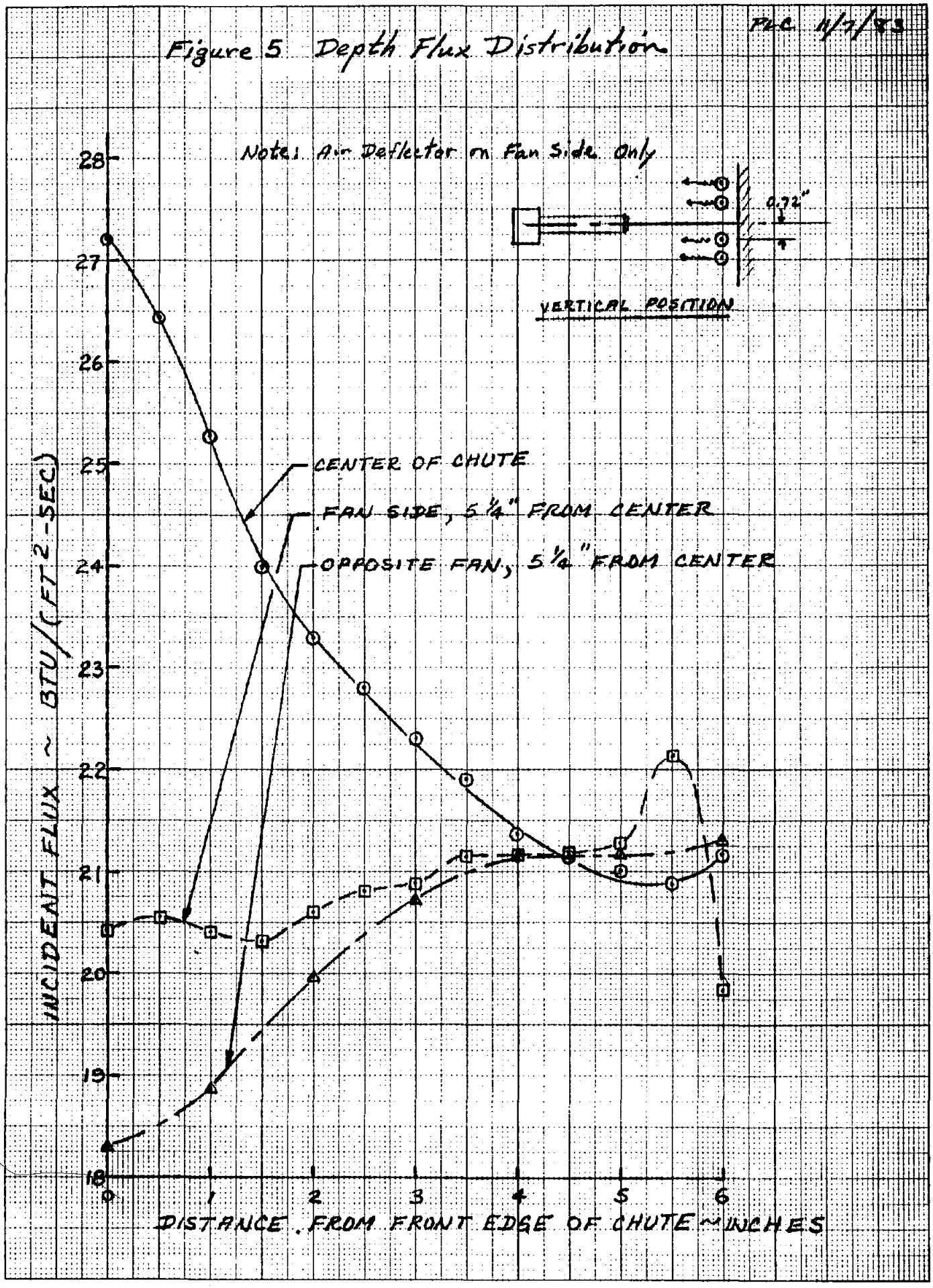
Figure 5 Depth Flux Distribution
PAC 11/7/83
Note: Air Deflector on Fan Side Only
0.72"
VERTICAL POSITION
CENTER OF CHUTE
FAN SIDE, 5 1/4" FROM CENTER
OPPOSITE FAN, 5 1/4" FROM CENTER
INCIDENT FLUX ~ BTU/(FT^2-SEC)
28
27
26
25
24
23
22
21
20
19
18
0
1
2
3
4
5
6
DISTANCE FROM FRONT EDGE OF CHUTE ~ INCHES

Figure 6 VERTICAL FLUX DISTRIBUTION

PLC 11/9/83

Note: Air Deflector on Fan Side Only

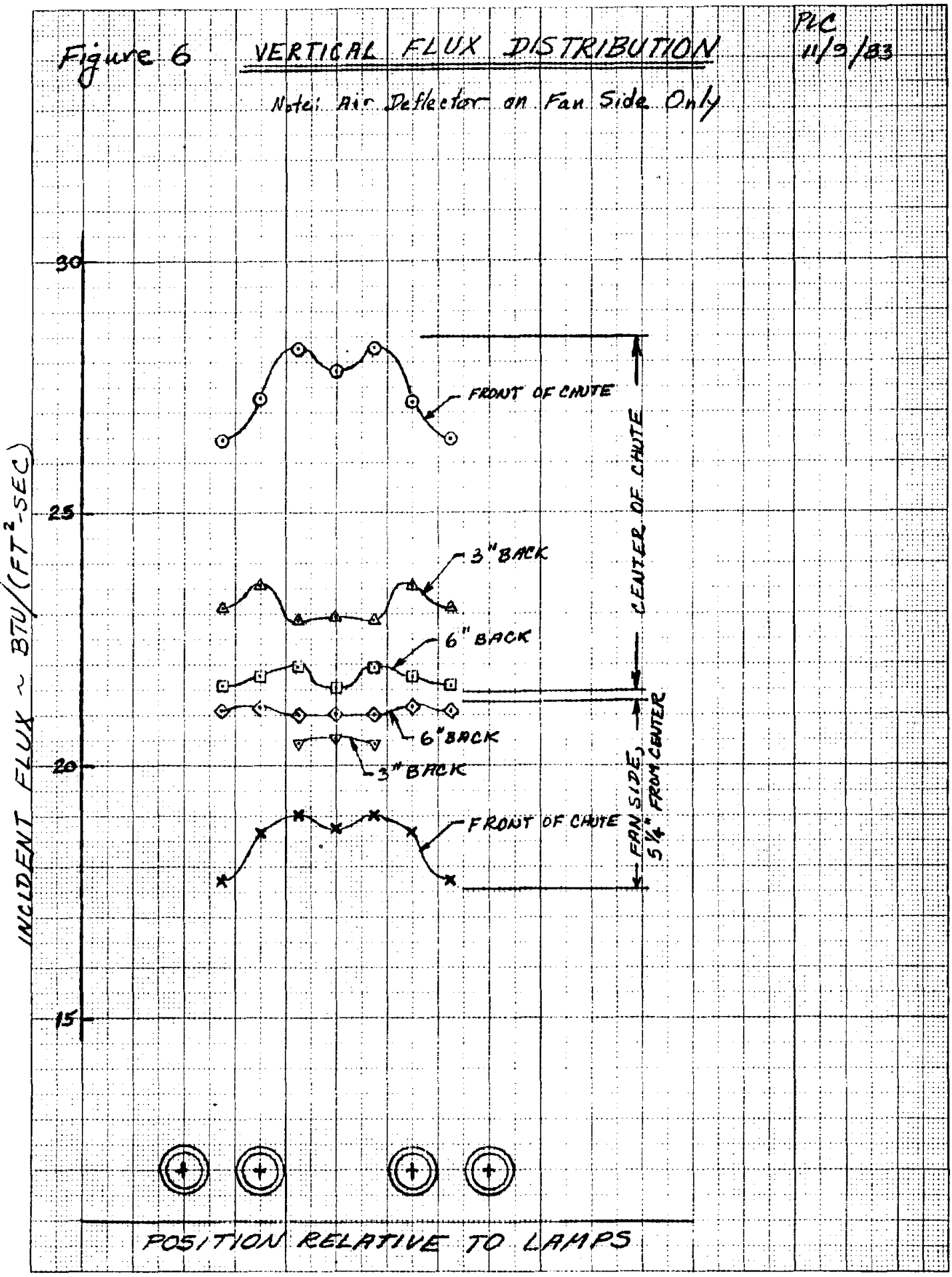

Figure 7 HORIZONTAL FLUX DISTRIBUTION

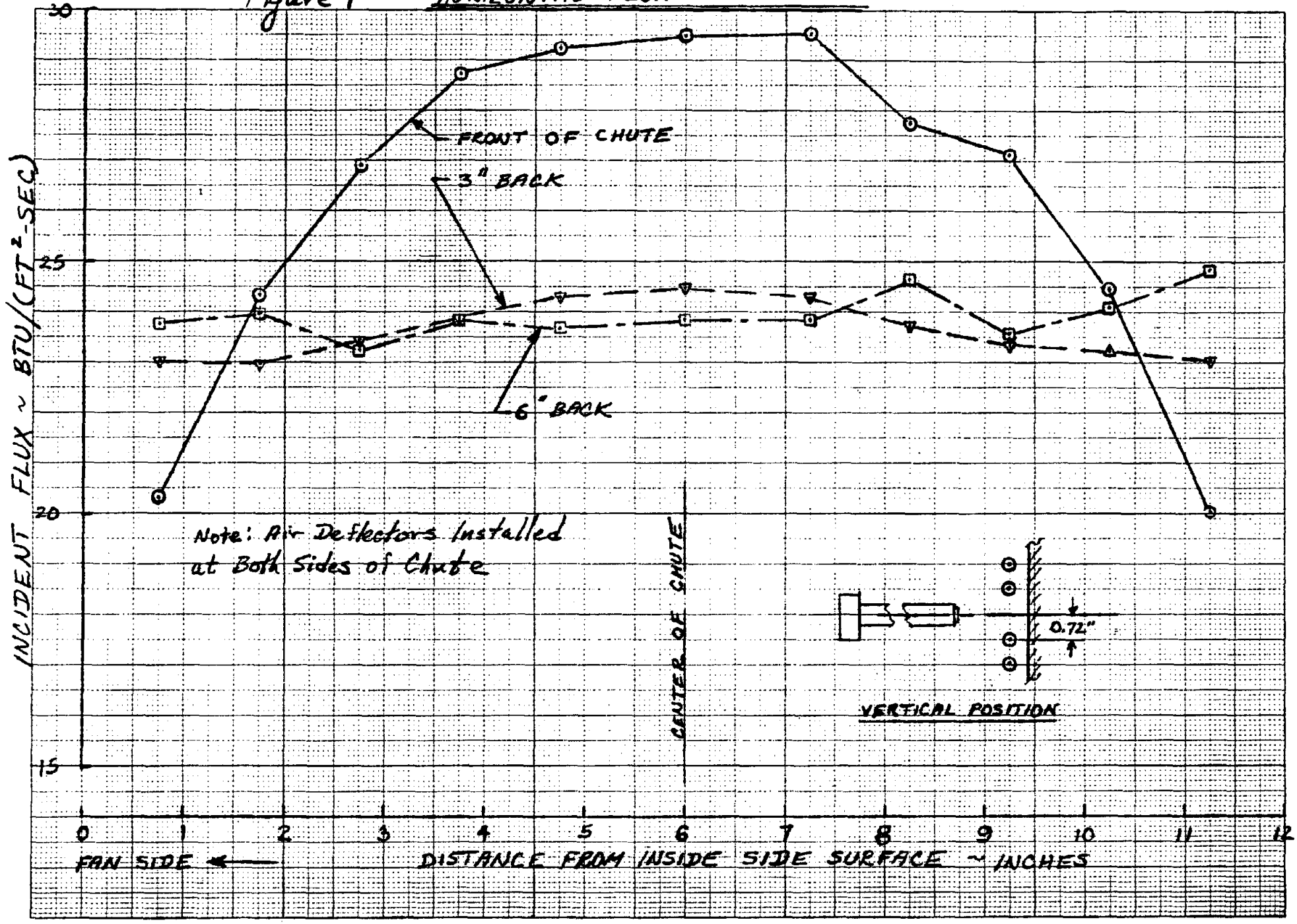

Sandia Laboratories

Albuquerque, New Mexico
Livermore, California

date: December 22, 1983

to: B. R. Steele, 8453

from: Jim Nakos
J. T. Nakos, 7531

subject: Flux Distribution Measurements

So that the flux distribution measurements in a typical chute section are more usable at different nominal flux levels, we took the raw data and normalized the values to the single highest value on each plot from the memorandum by P. L. Class on November 17, 1983.

The normalized depth, vertical and horizontal profiles are shown in Figures 1, 2 and 3, respectively. These curves directly correspond to the original curves in the aforementioned memo, except for the original curve on Figure 5 labeled, "opposite fan, 5 1/4 in. from center." This configuration is not used on the real setup since in that configuration the chute was not fully enclosed and therefore is not included in this data.

My thanks go to B. L. Hunt for helping with the data reduction.

JTN:7531:jp

Copy to:
7531 P. L. Class
7531 J. Gabaldon
7531 B. L. Hunt
7531 S. D. Taylor
8124 J. M. Hruby
8313 V. P. Burolla
7531 J. T. Nakos

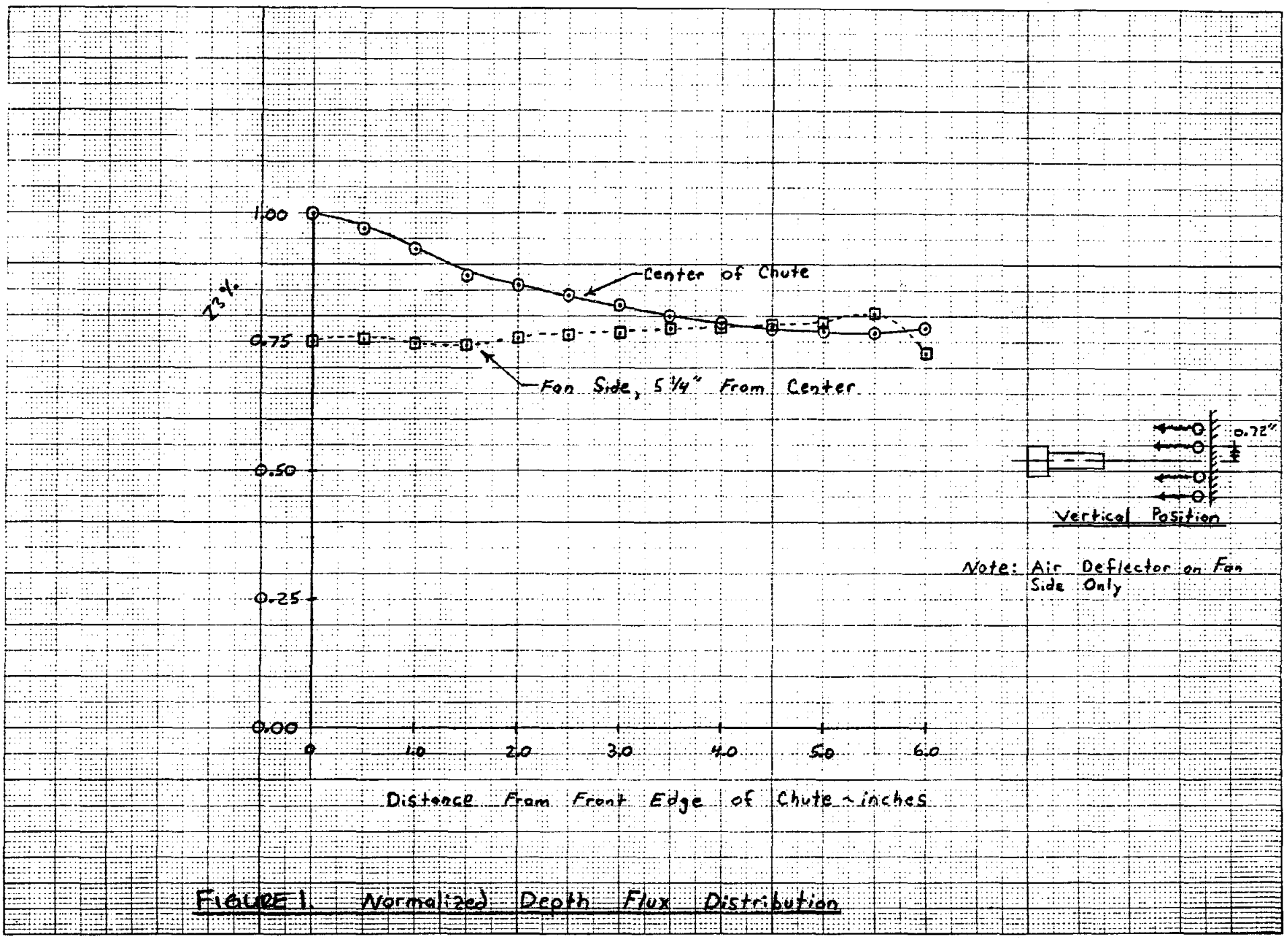

FIGURE 1. Normalized Depth Flux Distribution

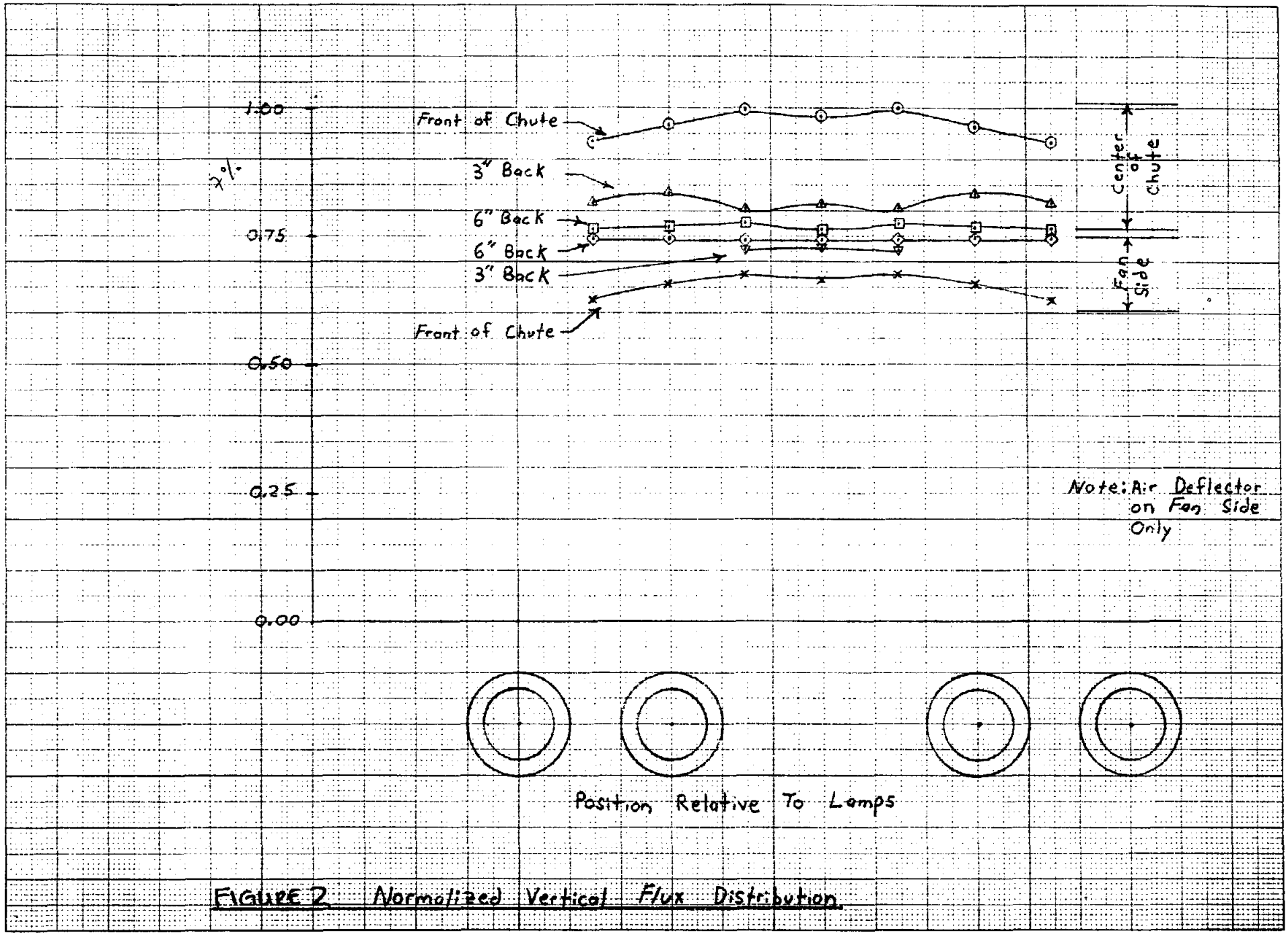

FIGURE 2 Normalized Vertical Flux Distribution.

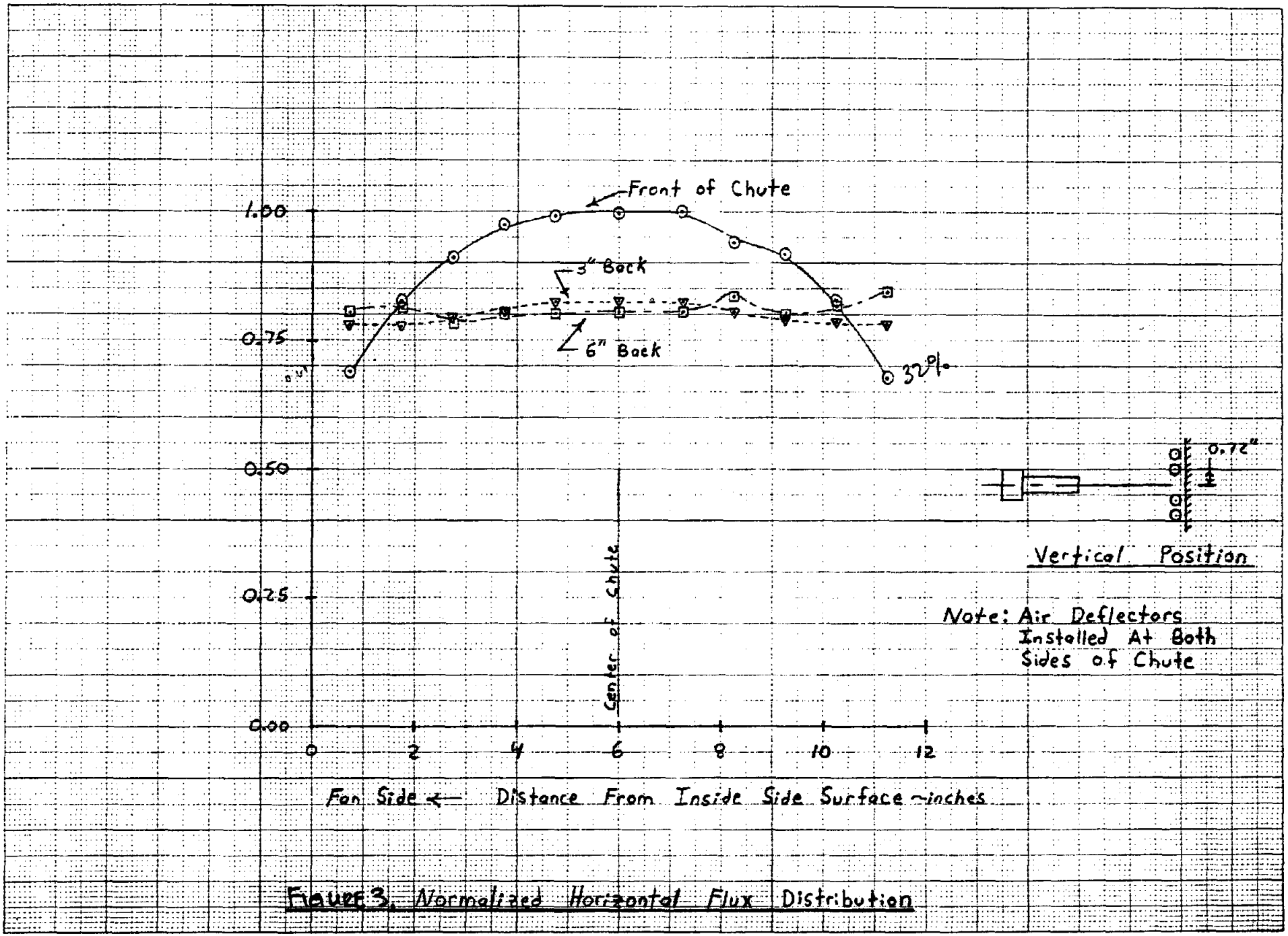

Figure 3. Normalized Horizontal Flux Distribution

REFERENCES

1. Falcone, P.K., J.E. Noring and C.E.Hackett, "Evaluation and Application of Solid Thermal Energy Carriers in a High Temperature Solar Central Receiver System," Proceedings of the 17th Intersociety Energy Conversion Engineering Conference, Vol.3, 1983.
2. Hruby, J. M., and V. P. Burolla, "Solid Particle Receiver Experiments: Velocity Measurements," SAND84-8238, Oct. 1984.
3. Messing, G. L. and D. M. Kupp, "Sintering of Coarse Ceramic Particulates," 1st Quarterly Report, Contract No. 31-5419, June 15, 1983.
4. Peskin, R. L. and R. Briller, Tech. Rpt. No. 109- ME- F NYO2930- 7 (Rutgers Univ., New Brunswick, New Jersey).
5. Siegel, R. and J. R. Howell, *Thermal Radiation Heat Transfer*, Second Edition, Hemisphere Publishing Corporation, 1981, Appendix D.
6. Touloukian, Y. S., ed., *Thermophysical Properties of Matter*, 1970.
7. Emery, A. F., "Instruction Manual for the Program SHAPEFACTOR," SAND80-8027, October 1980.
8. Abrams, M., "RADSOLVER - A Computer Program for Calculating Spectrally-Dependent Radiative Heat Transfer in Solar Cavity Receivers," SAND81-8248, September 1981.
9. Lajeunesse, C. A., "Thermal Performance of a Solid Particle Cavity Receiver and Related Phenomena," SAND Report, to be published.
10. Falcone, P. K., editor, "Technical Review of the Solid Particle Receiver Program January 25-26, 1984," SAND84-8229, July, 1984.
11. Bohren, C. F. and D. R. Huffman, *Absorption and Scattering of Light by Small Particles*, John Wiley & Sons, 1983, pp. 316-317.

UNLIMITED RELEASE INITIAL DISTRIBUTION:

U.S. Department of Energy (5)
Forrestal Building, Room 5H021
Code CE-314
1000 Independence Avenue, S.W.
Washington, D.C. 20585
Attn: C. Carwile
H. Coleman
C. Mangold
F. Morse
M. Scheve

U. S. Department of Energy (2)
P.O. Box 5400
Albuquerque, NM 87115
Attn: D. Graves
J. Weisiger

U.S. Department of Energy (2)
1333 Broadway
Oakland, CA 94612
Attn: T. Vaeth
R. Hughey

North Carolina State University
P.O. Box 7905
Chemical Engineering Department
Rayleigh, NC 27695
Attn: Prof. R. Carbonell

University of California
Department of Mechanical Engineering
6167 Etcheverry Hall
Berkeley, CA 94720
Attn: Prof. R. Greif

University of Houston
Solar Energy Laboratory
4800 Calhoun
Houston, TX 77704
Attn: Prof. A. Hildebrandt

Washington State University
Department of Mechanical Engineering
Pullman, WA 99164-2920
Attn: Prof. C. Crowe

Applied Aeroponics
7000 Village Parkway
Suite 1
Dublin, CA 94566
Attn: V. P. Burolla

Center for Materials Science
Inorganic Materials Division
National Bureau of Standards
Washington, D.C. 20234
Attn: S. M. Wiederhorn

Centre National De La Recherche Scientifique (2)
Laboratorie d'Energetique Solaire
Odiello, B.P. 5, 66120 Font- Romeu
France
Attn: G. Flamant
C. Royere

Electric Power Research Institute (2)
P.O. Box 10412
Palo Alto, CA 94303
Attn: J. Bigger
E. DeMeo

Electro-Optic Systems Section
Pacific Northwest Laboratories
Battelle Boulevard
Richland, WA 99352
Attn: J. W. Griffin

Solar Energy Research Institute (4)
1617 Cole Boulevard
Golden, CO 80401
Attn: M. Carasso
R. Copeland
B. Gupta
R. Hulstram

Southern California Edison (2)
P. O. Box 800
Rosemead, CA 92807
Attn: J. N. Reeves
P. Skvarna

Lawrence Berkeley Laboratories 90-2024
Berkeley, CA 94720
Attn: A. Hunt

Lawrence Livermore National Laboratory, L-200
Attn: O. R. Walton

R. B. Pettit, 1824
F. P. Gerstle, 1845
J. R. Hellmann, 1845
T. A. Michalske, 1845
E. H. Beckner, 6000; Attn: V. Dugan, 6200
D. G. Schueler, 6220
J. V. Otts, 6222
B. F. Blackwell, 7531
P. L. Class, 7531
S. T. Letourneau, 7531
S. D. Taylor, 7531

J. T. Nakos, 7533
N. R. Keltner, 7537

R. S. Claassen, 8000; Attn: D. M. Olson, 8100
A. N. Blackwell, 8200
D. L. Hartley, 8300

C. S. Selvage, 8000A

C. W. Robinson, 8240; Attn: G. A. Benedetti, 8241
M. L. Callabresi, 8242
M. R. Birnbaum, 8243
C. S. Hoyle, 8249

C. M. Hartwig, 8244
W. G. Houf, 8244
G. H. Evans, 8245
M. E. John, 8245
C. A. LaJeunesse, 8245

R. C. Wayne, 8400; Attn: L. D. Bertholf, 8430
H. Hanser, 8440
R. L. Rinne, 8470

J. B. Wright, 8450
P. K. Falcone, 8452
A. C. Skinrood, 8452
J. M. Hruby, 8453 (35)
G. H. Prescott, 8453
B. R. Steele, 8453
J. C. Swearengen, 8453
J. B. Wright, 8454 (actg.)
Publications Division, 8265, for TIC (27)
Publications Division, 8265/Technical Library Processes Division, 3141
Technical Library Processes Division, 3141 (3)
M. A. Pound, 8024, for Central Technical Files (3)